AUG 15 1991

AEDC-TR-91-2

C.3

Effect of Geometric Parameters on the Performance of Second Throat Annular Steam Ejectors

S. E. Stephens and L. B. Bates
Sverdrup Technology, Inc.

July 1991

Final Report for Period February 28 to September 30, 1990

TECHNICAL REPORTS
FILE COPY

PROPERTY OF U.S. AIR FORCE
AEDC TECHNICAL LIBRARY

Approved for public release; distribution is unlimited.

AEDC TECHNICAL LIBRARY
5 0720 00062 7077

ARNOLD ENGINEERING DEVELOPMENT CENTER
ARNOLD AIR FORCE BASE, TENNESSEE
AIR FORCE SYSTEMS COMMAND
UNITED STATES AIR FORCE

NOTICES

When U. S. Government drawings, specifications, or other data are used for any purpose other than a definitely related Government procurement operation, the Government thereby incurs no responsibility nor any obligation whatsoever, and the fact that the Government may have formulated, furnished, or in any way supplied the said drawings, specifications, or other data, is not to be regarded by implication or otherwise, or in any manner licensing the holder or any other person or corporation, or conveying any rights or permission to manufacture, use, or sell any patented invention that may in any way be related thereto.

Qualified users may obtain copies of this report from the Defense Technical Information Center.

References to named commercial products in this report are not to be considered in any sense as an endorsement of the product by the United States Air Force or the Government.

This report has been reviewed by the Office of Public Affairs (PA) and is releasable to the National Technical Information Service (NTIS). At NTIS, it will be available to the general public, including foreign nations.

APPROVAL STATEMENT

This report has been reviewed and approved.

PAUL LACASSE, Capt, CF
Facility Technology Division
Directorate of Technology
Deputy for Operations

Approved for publication:

FOR THE COMMANDER

KEITH L. KUSHMAN
Director of Technology
Deputy for Operations

REPORT DOCUMENTATION PAGE

Form Approved
OMB No. 0704-0188

Public reporting burden for this collection of information is estimated to average 1 hour per response, including the time for reviewing instructions, searching existing data sources, gathering and maintaining the data needed, and completing and reviewing the collection of information. Send comments regarding this burden estimate or any other aspect of this collection of information, including suggestions for reducing this burden, to Washington Headquarters Services, Directorate for Information Operations and Reports, 1215 Jefferson Davis Highway, Suite 1204, Arlington, VA 22202-4302, and to the Office of Management and Budget, Paperwork Reduction Project (0704-0188), Washington, DC 20503

1 AGENCY USE ONLY (Leave blank)	2 REPORT DATE	3. REPORT TYPE AND DATES COVERED
	July 1991	Final - 28 February - 30 September 1990

4. TITLE AND SUBTITLE
Effect of Geometric Parameters on the Performance of Second Throat Annular Steam Ejectors

5. FUNDING NUMBERS
PE - 65807F
PN - DD02EW

6. AUTHOR(S)
Stephens, S. E. and Bates, L. B., Sverdrup Technology, Inc., AEDC Group

7 PERFORMING ORGANIZATION NAME(S) AND ADDRESS(ES)
Arnold Engineering Development Center/DOT
Air Force Systems Command
Arnold Air Force Base, TN 37389-5000

8. PERFORMING ORGANIZATION REPORT NUMBER
AEDC-TR-91-2

9 SPONSORING/MONITORING AGENCY NAMES(S) AND ADDRESS(ES)
Arnold Engineering Development Center/DO
Air Force Systems Command
Arnold Air Force Base, TN 37389-5000

10 SPONSORING/MONITORING AGENCY REPORT NUMBER

11. SUPPLEMENTARY NOTES
Available in Defense Technical Information Center (DTIC).

12a DISTRIBUTION/AVAILABILITY STATEMENT
Approved for public release; distribution is unlimited.

12b. DISTRIBUTION CODE

13 ABSTRACT (Maximum 200 words)

Steam ejectors are simple pumps that, among many possible applications, are used in altitude simulation rocket motor testing. Of the two main types of ejectors, annular and centerbody, the latter has been the subject of most previous research. Less is known about the operation of annular ejectors. For example, ejector diffusers that contain a contraction known as a second throat have been studied widely for centerbody configurations; however, very little work has been conducted on second throat annular ejectors. An experimental study of second throat annular steam ejectors was conducted to determine the effects of specific design variables. The design variables investigated were second throat area ratio, location, and inlet ramp angle. The experimental results show that second throat area ratio has a strong impact on system operation, as expected. The second throat axial position appears to have a mild impact on the overall pressure recovery of the system over most of the range investigated, but with a strong effect when the second throat ramp is moved forward to the steam nozzle outlet. At this point, there is a large degradation in cell pressure. Ramp angle over the range investigated does not have a significant effect on cell pressure. A computational study was also conducted to evaluate the suitability of a single-phase Navier-Stokes computational fluid dynamics (CFD) code for prediction of steam ejector flow fields. The results of the study concluded that the state of the art (circa 1989) was insufficient for the successful prediction of ejector performance. The inability to model the condensation effects is indicated as a major cause of the deficiency.

14. SUBJECT TERMS
steam ejectors
computational fluid dynamics

15. NUMBER OF PAGES
70

16 PRICE CODE

17 SECURITY CLASSIFICATION OF REPORT	18 SECURITY CLASSIFICATION OF THIS PAGE	19 SECURITY CLASSIFICATION OF ABSTRACT	20. LIMITATION OF ABSTRACT
UNCLASSIFIED	UNCLASSIFIED	UNCLASSIFIED	SAME AS REPORT

COMPUTER GENERATED

Standard Form 298 (Rev. 2-89)
Prescribed by ANSI Std Z39-18
298-102

PREFACE

The work reported herein was conducted at Arnold Engineering Development Center (AEDC), Air Force Systems Command (AFSC), at the request of the AEDC Directorate of Technology. The results of the test program were obtained by Sverdrup Technology, Inc., AEDC Group, operating contractor for the propulsion test facilities at AEDC, AFSC, Arnold Air Force Base, Tennessee, under Project DD02EW. The Air Force project manager was Captain J. E. Paul Lacasse, Canadian Forces. The project manager for Sverdrup Technology was Samuel E. Stephens. The testing was completed on September 24, 1990. The original manuscipt was submitted on January 31, 1991, and a revised manuscript was submitted on May 14, 1991.

CONTENTS

Page

1.0 INTRODUCTION 7
2.0 TEST APPARATUS 9
2.1 Test Facility 9
2.2 Test Cell and Rocket Diffuser 9
2.3 Rocket Exhaust Gas Generator 10
2.4 Steam Ejector 10
2.5 Ejector Diffusers 10
2.6 Instrumentation 11
3.0 TEST DESCRIPTION 12
4.0 TEST RESULTS AND DISCUSSION 13
4.1 Baseline Configuration 14
4.2 Effect of Throat Location 18
4.3 Effect of Throat Contraction 20
4.4 Effect of Ramp Angle 21
5.0 APPLICATION OF COMPUTATIONAL TECHNIQUES TO EJECTOR PERFORMANCE PREDICTION 22
6.0 SUMMARY OF RESULTS 24
7.0 RECOMMENDATIONS 25
REFERENCES 25

ILLUSTRATIONS

Figure Page

1. Rocket Motor Altitude Test Facility 27
2. Second Throat Annular Steam Ejector 27
3. Test Configuration 28
4. BATES Solid-Propellant Rocket Motor 29
5. Steam Ejector Geometry 31
6. Test Instrumentation Locations 33
7. Instrumentation System Schematic 34
8. Typical Time Trace for Steam System Stabilization 35
9. Steam Ejector Rise Ratio Versus Normalized Total Pressure for Baseline Design 36
10. Steam Ejector Breakdown Curve for Baseline Design 37

Figure | Page

11. Hale and Gobbell's Annular Ejector Configurations (Ref. 9) 38
12. Comparison of Baseline to Data of Hale and Gobbell (Ref. 9) 39
13. Ejector Diffuser Exit Pitot Pressure Profiles 41
14. Normalized Cell Pressure versus Rake Average Exit Pitot Pressure 42
15. Baseline Wall Pressure Profiles 43
16. Effect of Secondary Flow on Miminum Cell Pressure 44
17. Rocket Test Results for Baseline at Low Steam and Exit Pressures—Started Diffuser 45
18. Rocket Test Results for Baseline at High Steam and Exit Pressures—Unstarted Diffuser 46
19. Rocket Test Results for Baseline at High Steam Pressure and Started Diffuser 47
20. Effect of Throat Location on Ejector Breakdown Curve 48
21. Effect of Throat Location on Maximum Rise Ratio 49
22. Effect of Throat Location on Wall Pressure Profile 50
23. Rocket Test Results for Configuration 5 at Low Steam and Exit Pressures—Started Diffuser 51
24. Rocket Test Results for Configuration 5 at High Steam Pressure and Started Diffuser 52
25. Rocket Test Results for Configuration 4 at High Steam Pressure and Started Diffuser 53
26. Effect of Contraction Ratio on Ejector Breakdown Curve 54
27. Effect of Contraction Ratio on Maximum Rise Ratio 55
28. Effect of Contraction Ratio on Wall Pressure Profile 56
29. Rocket Test Results for Configuration 6 at Low Steam and Exit Pressures—Started Diffuser 57
30. Rocket Test Results for Configuration 6 at High Steam Pressure and Started Diffuser 58
31. Effect of Ramp Angle on Ejector Breakdown Curve 59
32. Effect of Ramp Angle on Maximum Rise Ratio 60
33. Effect of Ramp Angle on Wall Pressure Profile 61
34. Rocket Test Results for Configuration 7 at High Steam Pressure and Started Diffuser 62
35. Analytical Code Calibration Results 63

TABLES

Tables | Page

1. Ejector Configurations 63
2. Measurement Uncertainties 64
3. Ejector Performance Summary 65
4. Point Correlation for Figures 9-10, 13-15 65

NOMENCLATURE 66

1.0 INTRODUCTION

An ejector is a simple pump. It uses a high-pressure primary flow to pump, by jet mixing, a secondary flow from a low-pressure environment to a higher backpressure. One application of an ejector, shown in Fig. 1, is in a rocket motor altitude test facility. Here the ejector is used to obtain low test cell pressures to simulate altitude conditions at motor ignition and to help prevent the rocket exhaust flow from blowing back into the test cell at motor burnout. In this application steam is often used for the ejector primary gas.

A steam ejector comprises one or more supersonic steam nozzles and a diffuser. The nozzles provide a high-pressure, high-momentum stream of gas that expands in the diffuser duct. During the expansion, flow is entrained from a secondary source by jet mixing, resulting in a kinetic energy transfer from the primary (steam) flow to the secondary flow (Ref. 1). The diffuser slows the mixed flow, converting the kinetic energy into increased static, or recovered, pressure. The net result is the pumping of the low static pressure secondary flow to a higher static pressure.

An ejector can operate at either started or unstarted conditions. At low ratios of backpressure to steam pressure the ejector will operate started. In this case, the flow expands to fill the diffuser duct with supersonic flow across the diameter of the duct. Because the flow is supersonic, the pressure at the secondary flow inlet is independent of the diffuser exit pressure. If there is no net secondary flow, the cell pressure for a started ejector is a function of the ejector geometry and driving pressure. At higher pressure ratios the diffuser will be unstarted. The flow does not fill the diffuser so there is a subsonic layer to transmit the pressure upstream. Therefore, the cell pressure is also a function of the diffuser exit pressure for an unstarted ejector. The critical ratio of exit to steam pressure that determines whether the system is started or unstarted is referred to as the breakdown pressure.

During the rocket motor firing, the motor and the rocket diffuser can operate together as another ejector. If this 'ejector' is started, the test cell pressure will be a function of the rocket motor and the diffuser geometry. As with the steam ejector, the rocket diffuser exit pressure must be less than its breakdown pressure for it to be started. The steam ejector must be compatible with the rocket diffuser such that it does not prevent starting of, or unstart, the rocket diffuser.

As noted by Lewis and Drabble (Ref. 2), "Ejectors are normally classified according to the type of primary nozzle used, either annular or central; the annular nozzle being located at the periphery of the mixing tube and the central nozzle along the axis." Lewis and Drabble pointed out that the central nozzle configuration tends to provide better performance than the annular in terms of minimum test cell pressure. However, the annular configuration is

frequently preferred for rocket altitude testing because the steam ejector body and nozzle are not immersed in the harsh rocket exhaust flow, thus reducing the need for elaborate cooling and frequent maintenance.

By varying nozzle and/or diffuser geometry, many ejector configurations are possible. One such configuration shown in Fig. 2 is an annular ejector in which the diffuser contains a contraction, or second throat. Second throat ejectors have an advantage over straight diffusers because the second throat increases the pressure recovery of the system (Ref. 3).

Second throat ejectors have been studied in the past (e.g., Refs. 3-10) but only to a limited extent. Most of the previous work has focused on second throats for central ejectors. There has only been a little work with annular second throat ejectors (e.g., Refs. 9-10). Furthermore, the studies conducted for annular ejectors have been examinations of a few specific geometries, rather than systematic studies. Thus, the effects of individual design parameters on system operation have not been investigated for annular second throat ejectors.

The aim of the research reported herein was to broaden the base of knowledge concerning second throat annular steam ejectors. More specifically, the goal of the current study was to evaluate the effects of some individual geometric design variables on ejector operating characteristics, including minimum cell pressure and the pressure rise across the ejector diffuser system.

Because of the range of possible configurations, it is not practical to characterize the parametric effects for all second throat annular configurations. The work reported herein focused on one particular ejector design, hereafter referred to as the baseline, and the effects of the individual second throat diffuser design parameters.

The parametric effects were determined by conducting an experimental study. A baseline second throat annular steam ejector was fabricated and tested to establish benchmark performance. Then alternate ejectors that varied from the baseline in one variable were evaluated to determine the contribution of the changed variable. These alternate configurations varied either the location (L_d), the area ratio (A_{st}/A_d), or the ramp angle (Θ) of the second throat.

The experimental study is described in Sections 2.0 through 4.0. Section 2.0 provides a detailed description of the test apparatus, and Section 3.0 discusses the methods and procedures used during the testing. The experiment results are discussed in Section 4.0.

To complement the experiments, a computational study was performed to evaluate the ability of a single-phase, ideal gas, Navier-Stokes computational fluid dynamics (CFD) code

to predict steam ejector performance. A successfully calibrated computational tool would be valuable for future ejector studies. The current computational study applied a state-of-the-art (circa 1989) Navier-Stokes CFD code to a second throat annular steam ejector configuration for which experimental data were available. This configuration is slightly different from the present experimental configuration, but was considered sufficiently similar to provide a basis for calibration. The results of this application are presented in Section 5.0.

Section 6.0 summarizes the major results of the current study, and Section 7.0 offers recommendations for future research.

2.0 TEST APPARATUS

The testing reported herein was conducted at the Arnold Engineering Development Center (AEDC) in the Engine Test Facility (ETF) Research Test Cell T-6. Figure 3 is a sketch of the test installation. The test hardware consisted of a second throat annular steam ejector along with a model test cell, rocket diffuser, and a transition duct to interface between the test apparatus and the ETF exhaust system. Support systems included a steam supply and a nitrogen purge system. Rocket exhaust products were generated using small solid-propellant rocket motors. Additional secondary flow effects were evaluated using air inbleed ports built into the test cell.

2.1 TEST FACILITY

The ETF Research Test Cell T-6 is a propulsion development test cell designed for the investigation of rocket exhaust plume characteristics. The facility steam supply system can deliver saturated steam to T-6 at pressures up to 200 psia. The test cell is supported by a facility exhaust system capable of providing subatmospheric pressures as low as 0.5 psia. The exhaust system also includes a water spray chamber for cooling and condensation of the combined steam/rocket flow. Because rocket motors typically contain significant quantities of combustible species, the exhaust system also has the ability to add sufficient quantities of nitrogen to inert the flow.

2.2 TEST CELL AND ROCKET DIFFUSER

A test cell was included in the apparatus to house the rocket exhaust gas generator and provide a location for reference cell pressure measurements. Addy (Ref. 11) found that the cell geometry does not affect the steady-state cell pressure but, as expected, the test cell volume does affect the time required to obtain steady conditions, or response time, after a change in the ejector operating condition. Therefore, the test cell was designed to permit the system to reach equilibrium conditions during the rocket burn time, rather than represent a typical rocket altitude test cell.

Two air inbleed ports were built into the test cell to accommodate venturi nozzles for metering the secondary, or bleed, flows into the test cell. The venturi throat diameters were 1.313 and 1.570 in. Flow through the venturis was controlled in an on/off manner using rubber stoppers. The venturi air flows were used to evaluate secondary flow effects on the operation of the ejector.

The test hardware included a rocket diffuser which was of a second throat design. A rocket diffuser was needed to properly represent the geometry for the interaction of the primary steam flow and the secondary cell flow as in a typical rocket test cell application.

2.3 ROCKET EXHAUST GAS GENERATOR

The Ballistic Test and Evaluation System (BATES) solid-propellant rocket motor was selected to generate a rocket exhaust flow. A set of these motors was obtained from the Air Force Phillips Lab (OLAC/PL). The BATES motor shown in Fig. 4 used a propellant cartridge and a graphite nozzle, both of which were replaced after each firing. Other major components included the forward and aft closures, case, nozzle retaining ring, and nozzle extension skirt. The extended nozzle had an exit-to-throat area ratio of 96. All of these components were fabricated out of mild steel and were reusable. The propellant consisted of an ammonium perchlorate (AP) oxidizer and a hydroxy-terminated polybutadiene (HTPB) binder with aluminum fuel. The propellant aluminum loading was approximately 20 percent by weight. Nominal thrust for the motors was 2,000 lbf and nominal burn time was 2.4 sec.

2.4 STEAM EJECTOR

The annular steam ejector consisted of a nozzle/manifold assembly located around the annulus of, and near the exit of, the rocket diffuser. The steam ejector nozzle/manifold assembly, shown in detail in Fig. 5, consisted of a steam manifold fed by a supply line with a control valve, and 24 two-dimensional supersonic steam nozzles. The nozzle details are also shown in Fig. 5. This configuration is more accurately referred to as a segmented annular ejector as opposed to a pure annular ejector.

2.5 EJECTOR DIFFUSERS

Seven different ejector configurations were obtained by use of different ejector diffusers. This section discusses the baseline and alternate diffuser configurations that were tested.

2.5.1 Baseline Design

The baseline ejector diffuser employed a second throat configuration with the throat inlet ramp located one diameter downstream of the ejector nozzle exit plane (Table 1). The throat

ramp angle was 5 deg and the diffuser throat contracted to an area ratio of 81 percent relative to the largest diameter section of the diffuser.

The ejector diffuser exited into a larger diameter transition duct as shown in Fig. 3. The transition duct extended 1 diameter downstream and ¾ diameter upstream from the ejector diffuser exit plane. The assembly was attached to the T-6 exhaust duct and subsequently into the ETF exhaust plant. The transition duct provided the access for a diffuser exit plane pitot pressure rake.

2.5.2 Alternate Configurations

Six alternate ejector diffuser configurations were tested. A summary of the configurations is given in Table 1. The alternate configurations determined the effects of individual design parameters on system performance. The relative results from Configurations 2 through 5 (L_d/D_d = 0, 0.333, 0.667, and 1.333) and the baseline were used to determine the effect of second throat position. Configuration 6 (A_{st}/A_d = 0.7) and the baseline configuration were used to define the effect of contraction ratio, and Configuration 7 (Θ = 6.5 deg) and the baseline configuration were used to determine ramp angle effect.

2.6 INSTRUMENTATION

Instrumentation locations and parameter names are shown in Fig. 6. The major parameters of interest were test cell pressure, ejector total (manifold) pressure and temperature, ejector diffuser backpressure, and exit pitot pressure profiles. The system exit pressure was measured with three pressure transducers located downstream of the ejector diffuser: two measurements in the transition duct and one in the T-6 exhaust duct. Additionally, 27 pressures were recorded along the walls of the diffusers to help characterize the flow. The ejector diffuser exit pitot pressure was measured with a 6-probe pitot pressure rake. The six probes were set radially from the duct centerline on equal areas.

All pressures were measured using individual bonded, strain-gage-type pressure transducers, close-coupled to the model. The steam temperature was measured using a Chromel® -Alumel® thermocouple. Instrument system calibrations performed during the testing are traceable to the National Institute of Standards and Technology (NIST). Each link in the traceability chain to the NIST is maintained and documented by the AEDC Precision Measurement Equipment Laboratory (Ref. 12). Uncertainties for each of the parameters were calculated as described by Thompson and Abernathy (Ref. 13) and are given in Table 2.

Figure 7 is a schematic of the data acquisition process. The analog signals from the instrumentation were scanned and filtered using a front-end data system. The data were

digitized, processed using an SEL 3227 or 3277® computer, and then recorded on digital tape for offline processing. Final offline processing was done using the AEDC Amdahl 5860® Central Computer. The analog signals were also recorded on FM tape as backup and diagnostic tools in case of failure. Test conditions including steam driving pressure and temperature, test cell pressure, and transition duct static pressure were monitored online in the control room via a display readout from the SEL computer.

3.0 TEST DESCRIPTION

This section discusses the procedures and methodology used during the testing. The same procedures, except as noted, were used for each test to minimize biasing the results of one test relative to another.

Two types of testing were conducted: steam without rocket exhaust and steam with rocket exhaust. For simplicity, these are referred to herein as steam tests and rocket tests, respectively. Many of the test procedures were common to both types of tests. First, all instruments that were in operating range at the ambient conditions were calibrated *in situ*. Following this, the test apparatus was pumped down to approximately 0.5 psia using the ETF exhaust plant. The remaining low-range pressure transducers were then calibrated using a NIST secondary standard.

After the instrumentation calibration discussed above, a facility isolation valve downstream of the test apparatus was closed to perform a leak check. This was accomplished by measuring the static pressure in the test cell as a function of time and relating it to the potential inbleed, or leak, mass flow by the following equation:

$$\dot{m} = \frac{V}{RT} \frac{\delta P_{cell}}{\delta t} \tag{1}$$

where

$\dot{m}$ = Mass flowrate of inleakage,
V = Volume of the test apparatus upstream of the valve,
δP_{cell} = Cell pressure variation,
R = Gas constant for the air,
T = Ambient air temperature, and
δt = Elapsed time after valve closing.

Equation (1) does assume a constant temperature and zero leakage across the isolation valve. The measured leak rates were approximately 2.5 percent of the minimum steam flow

rates used during the tests. This leak rate is for all of the facility ducting upstream of the isolation valve. The test hardware, especially the test cell, which is the most sensitive to leakage, made up only a small fraction of the total ducting surface area. Although it cannot be quantified, it is believed that the leakage in the test cell was not large enough to affect the cell pressure during most of the tests. Tests with suspected larger leakages are noted in the presentation of results.

Following the air inleak check, the steam flow was started and set at a driving pressure high enough to ensure that the ejector was started. The steam flow was maintained at this level while the steam system warmed up. Stabilization was monitored by tracking normalized cell pressure, P_{cell}/P_{tst}, versus time as shown in Fig. 8. Typical stabilization time for a test was 20 min. This procedure was not followed for the first test. The data obtained from the first 20 min of the first test were unsteady and deviated from the remainder of the test data. The lack of prior stabilization was identified as the cause. To prevent a recurrence of the problem, the above procedure was adopted for the remaining tests. The suspect initial data from the first test are not included in the results reported herein.

Next, the desired backpressure was set using the plant exhaust machinery. Testing was then conducted with a matrix of various steam ejector driving pressures and diffuser exit pressures. Secondary flow was introduced using the inbleed venturis for several points within the test matrix. Steady-state data points were acquired at each flow condition.

Rocket tests began with verification of no stray voltage in the motor ignition system, followed by loading of the rocket motor in the test cabin. The calibration and thermal stabilization procedures were then executed as in the steam tests. Next, a GN_2 purge sequence was required to replace as much air (oxygen) as possible with nitrogen to preclude the presence of a combustible mixture within the exhaust system. At 150 sec before ignition, the steam pressure was increased to the desired level for firing. Also, the exhaust duct pressure was increased at this time to the desired test condition. Recording on the digital data acquisition system was initiated 30 sec prior to ignition, followed by arming of the rocket motor. Ten seconds before ignition, the cell GN_2 was turned off to eliminate secondary flow in the test cabin. The motor was then fired. Upon motor burnout, the test cell purge nitrogen flow was resumed. After 260 sec, the purge flow was stopped, and test shutdown procedures were initiated.

4.0 TEST RESULTS AND DISCUSSION

The results from the experimental program are presented first for the baseline configuration. These results are subdivided into steam test and rocket test results. Following the baseline results, the effects of individual parameter variation are detailed. As with the

baseline, these results are subdivided into steam and rocket test results. A summary of the results is presented in Table 3.

4.1 BASELINE CONFIGURATION

4.1.1 Steam Tests

The results for the baseline ejector were taken from two test periods. The first test was conducted in February 1990, while the latter test was conducted in September 1990.

The baseline results with no secondary flows are summarized in Figs. 9 and 10 and also in Table 3. The figures represent two common methods of presenting ejector performance data (Ref. 14). Figure 9 shows the ejector performance in terms of diffuser pressure rise ratio, P_{ex}/P_{cell}, versus steam driving pressure normalized by exit pressure, P_{tst}/P_{ex}. A maximum rise ratio of 12 was obtained for the baseline at a normalized total pressure of 28. The two tests show a slight difference in the results. The February test data have more scatter and a slightly higher average rise ratio than the September test data. A possible explanation for this is the variation of steam quality from season to season. However, this cannot be verified with the current data because steam quality was not measured. The five data points labelled A-E are reference points to relate Fig. 9 with some of the figures to be discussed below.

Figure 10 is a diffuser breakdown curve that plots cell pressure against exit pressure with both terms normalized by the steam total pressure. The curve shows that, for the baseline, the ejector is started, that is, the cell pressure is independent of exit pressure, for values of normalized exit pressure (P_{ex}/P_{tst}) below 0.036. The normalized cell pressure, P_{cell}/P_{tst}, for started operation was either 0.0030 or 0.0032, depending on the test. The former value corresponds to the winter test, while the latter value corresponds to the summer test. If the hypothesis that the only significant difference between the two tests was delivered steam quality is true, then Fig. 10 indicates that the steam quality has an effect on cell pressure.

Ratios of measured parameters to ideal calculations can be used to evaluate a configuration, or to compare it with other configurations. The one-dimensional, ideal gas, isentropic flow equations are used to calculate the theoretical minimum cell pressure that could be obtained by a given ejector configuration. The theoretical minimum value is defined as the one-dimensional isentropic static-to-total pressure ratio corresponding to the ratio of initial diffuser area to ejector nozzle throat area, A_d/A^*. This pressure is referred to as the isentropic cell pressure ratio, and is denoted $(P/P_t)_{isen}$. The resulting ratio of normalized cell pressure to isentropic cell pressure is denoted K_{isen} as given in Eq. (2).

$$K_{isen} = \frac{P_{cell}/P_{tst}}{(P/P_t)_{isen}} \tag{2}$$

A ratio of specific heats, γ, of 1.3 is often used for superheated steam in the ideal gas equations. Using this value and the baseline A_d/A^* of 40.08 yields an isentropic cell pressure of 0.0014 and a K_{isen} of 2.14 (for $P_{cell}/P_{tst} = 0.0030$).

As with the cell pressure, a theoretical maximum exit pressure can be calculated and used as a reference. The maximum exit static-to-driving pressure ratio is referenced to the ratio of downstream static pressure to upstream total pressure across a normal shock, $(P_2/P_{t1})_{ns}$. The resulting actual-to-ideal ratio, denoted K_{ns} is given by Eq. (3) in one-dimensional flow for an area ratio equal to the diffuser exit-to-nozzle throat area ratio.

$$K_{ns} = \frac{P_{ex}/P_{tst}}{(P_2/P_{t1})_{ns}} \tag{3}$$

Application of the ideal gas normal shock relations to the current baseline configuration yields a $(P_2/P_{t1})_{ns}$ of 0.0457 and a K_{ns} of 0.79. These calculations are based on a γ of 1.3.

A comparison of the baseline ejector system is made with a second throat annular steam ejector tested by Hale and Gobbell (Ref. 9), shown in Fig. 11 as Configuration 11a. Hale and Gobbell also tested a straight diffuser version of the same ejector, Configuration 11 in Fig. 11. The current baseline is compared to both of these configurations in Fig. 12. Figure 12a shows the started cell pressure as a function of diffuser-to-ejector throat area ratio, A_d/A^*. The isentropic cell pressure line for $\gamma = 1.3$ is also shown as a reference. Both of the Hale and Gobbell configurations had the same cell pressure, indicating that, as expected, diffuser geometry downstream of the initial steam plume expansion had little to no impact on the cell pressure. The baseline has a K_{isen} that is 21 percent higher, that is 21 percent farther above the isentropic line than the Hale data. This indicates that other parameters that were different between the two Hale and Gobbell configurations and the baseline have a significant effect. Two significant differences between the two designs, as shown in Figs. 5 and 11, were: (1) the nozzle exit-to-diffuser area ratio was 12 and 16.62 for the baseline and the Hale configurations, respectively, and (2) the baseline configuration had a segmented nozzle while the Hale configuration had a continuous annular nozzle. Sufficient information was not available to separate the effects of these differences.

The normalized exit pressure at breakdown for the baseline and the Hale and Gobbell configurations is shown in Fig. 12b as a function of the diffuser exit-to-nozzle throat area ratio. Hale and Gobbell's straight diffuser started at a normalized exit pressure of 0.0224, which is 62 percent of the normal shock pressure ratio for that area ratio. Hale and Gobbell

reduced the diffuser exit-to-throat area ratio by 62 percent, which increased the starting exit pressure ratio by 52 percent to 0.034. However, the ideal normal shock recovery also increased. The net result was that the second throat achieved 60 percent of the normal shock recovery, nearly the same as the straight diffuser version.

The current baseline second throat had a starting exit pressure ratio of 0.036, or 79 percent of its corresponding normal shock value. This is a significantly higher percentage than either of the Hale and Gobbell configurations. The difference is most likely attributable to the fact that the baseline diffuser was more than 60 percent longer, in terms of exit diameters, than Hale and Gobbell's second throat diffuser, and twice as long as the straight diffuser.

Ejector systems sometimes display hysteresis in their operation; i.e., the pressure ratio at which the ejector starts is less than that at which it breaks down. In the current study, no evidence of hysteresis could be seen in the steady-state data. Several attempts to measure it were made by taking transient data points while varying the driving pressure and holding the exit pressure constant. The results were inconclusive because of the volume dynamics and the lack of precise transient control of the steam pressure.

A pressure rake at the diffuser exit provided profiles of pitot pressure measurements. The profiles for five data points are shown in Fig. 13 with the pitot pressure normalized by the ejector exit static pressure $P_{tex\text{-}n}/P_{seex}$. Also shown in Fig. 13 is a line at $P_{tex\text{-}n}/P_{seex}$ of 1.83 that represents the $\gamma = 1.3$ one-dimensional ideal gas pitot pressure for sonic velocity (Mach = 1) flow. Values of $P_{tex\text{-}n}/P_{tst}$ to the left of this line represent subsonic flow while values to the right represent supersonic flow. The profiles of Fig. 13 show that when the diffuser is unstarted (Curves D and E), the exit pitot profiles are subsonic and flat. When the diffuser starts (Curves A, B, and C), the profiles become highly nonuniform with a supersonic core. Also, observations during testing showed that the pitot pressures were very unsteady when the diffuser was started.

The rake pressures were area-averaged, normalized by steam driving pressure, and plotted against the normalized cell pressure. The resulting data are shown in Fig. 14. Comparison with the breakdown curve of Fig. 10 shows that the unstarted leg of the curve is similar for both figures. This is expected, since the exit pitot and static pressures are nearly the same in the unstarted regime. However, for the started diffuser, the exit pitot pressure increases faster than the driving pressure and the curve moves to higher values of P_{tex}/P_{tst}. The curve shows that the normalized cell pressure is a double-valued function of the pitot pressure ratio.

In addition to the exit rake measurements, several wall pressure measurements were also taken. Wall pressure profiles for the baseline are shown in Fig. 15. The wall pressures in Fig. 15 are normalized by the steam driving pressure. The figure shows that cell pressure

ERRATA

AEDC-TR-91-2, July 1991

EFFECT OF GEOMETRIC PARAMETERS ON THE PERFORMANCE OF SECOND THROAT ANNULAR STEAM EJECTORS

S. E. Stephens and L. B. Bates
Sverdrup Technology, Inc., AEDC Group

Arnold Engineering Development Center
Air Force Systems Command
Arnold Air Force Base, TN 37389-5000

Approved for public release; distribution is unlimited.

Figure 17 and Table 2 of the subject report were reproduced incorrectly. The corrected figure and table are included on this page.

Table 2. Measurement Uncertainties*

Parameter	Description	Bias (B)	Precision (S)	Uncertainty† (U)	Range
Pcell1	Test cell pressure	±0.036 psia	±0.0017 psia	±0.007 psia	0.15 to 1.5 psia
Pcell2	Test cell pressure	±2.0	±1.0	±4.0	0.5 to 3.0 psia
Pcell3	Test cell pressure	±1.4	±0.3	±2.0	2 to 15 psia
Pwall1 - Pwall6	Rocket diffuser wall static pressure	±0.035 psia	±0.0075 psia	±0.05 psia	0.5 to 3.0 psia
Pwall7 - Pwall13	Ejector diffuser wall static pressure	±2.0	±1.0	±4.0	0.5 to 3.0 psia
Pwall14 - Pwall17	Ejector diffuser wall static pressure	±2.0	±1.0	±4.0	1 to 5 psia
Pwall18 - Pwall27	Ejector diffuser wall static pressure	±1.4	±0.3	±2.0	2 to 15 psia
Pseex	Ejector diffuser exit wall static pressure	±1.4	±0.3	±2.0	2 to 15 psia
Ptex1 - Ptex6	Ejector diffuser exit pitot pressure	±1.4	±0.3	±2.0	2 to 15 psia
Pduct1 - Pduct2	Transition duct wall static pressure	±1.4	±0.3	±2.0	2 to 15 psia
Pduct3	Exhaust duct static pressure	±1.4	±0.3	±2.0	2 to 15 psia
Ptst1 - Ptst2	Steam manifold pressure	±1.4	±0.3	±2.0	50 to 210 psia
Ptc1, Ptc2	Rocket motor chamber pressure	±2.0 ±10 psia	±1.0 ±5 psia	±4.0 ±20 psia	500 to 2,000 psia <500 psia
Ttst	Steam manifold temperature	±(0.8°F + 0.38 percent Reading)	±0.6°F	±(2.0°F + 0.38 percent Reading)	240 to 400°F

* Bias, precision, and uncertainty are all percent of reading unless otherwise noted.

† $U = (B + t_{95}S)$

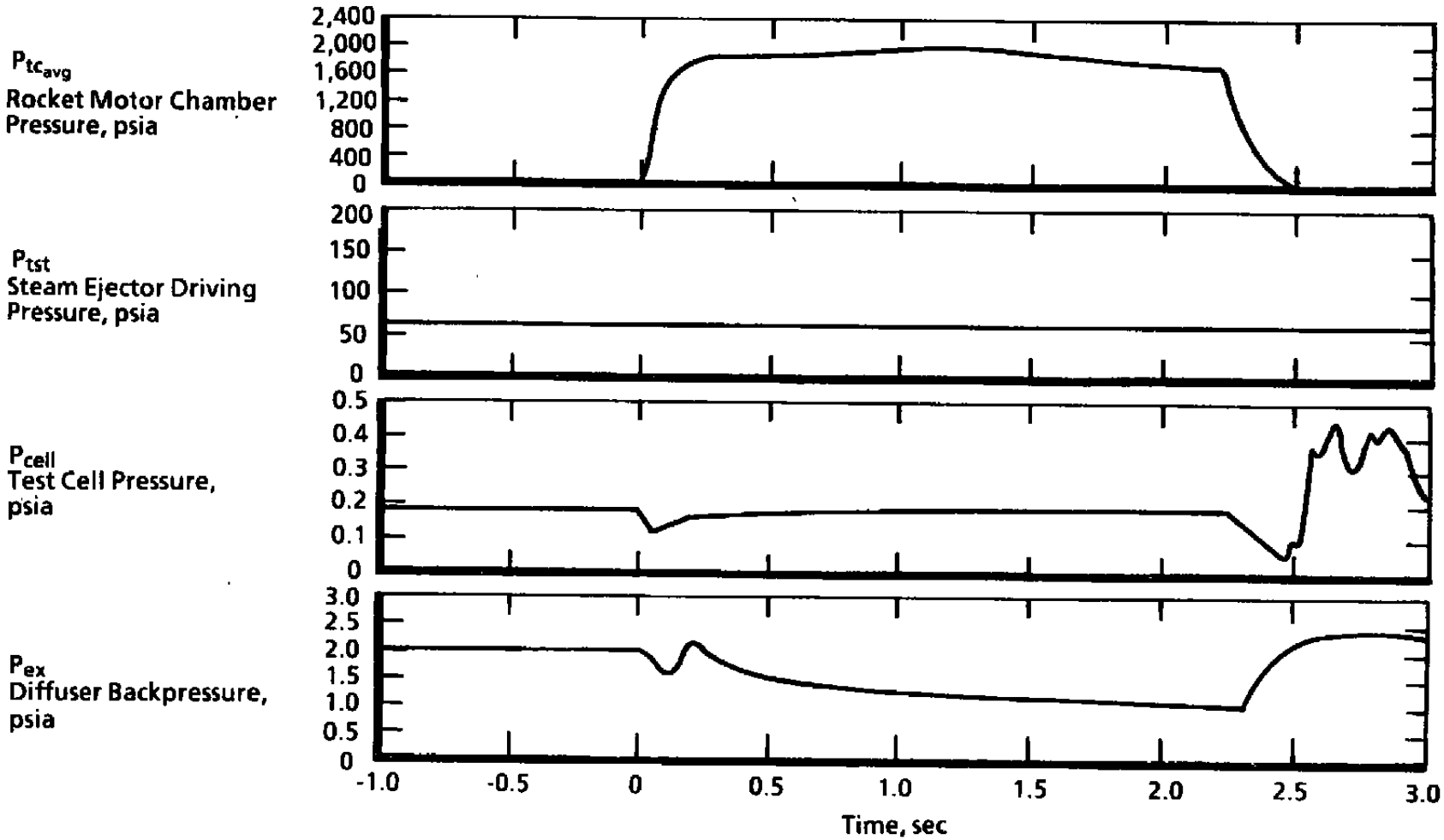

Figure 17. Rocket test results for baseline at low steam and exit pressures—started diffuser

(Axial Distance = −2) remains constant as P_{ex}/P_{tst} increases, from 0.011 to 0.033, indicating that the system is started. For values of P_{ex}/P_{tst} greater than 0.033, cell pressure increases, indicating that the system is unstarted. Figures 9-10 and 13-15 can be used together to relate different parameters at similar conditions. Figure 9 shows five points, labelled A through E. These same points are also shown in Figs. 10, 13, and 14. The wall pressure profiles of Fig. 15 include five curves labelled A through E. Each of these curves corresponds to the similarly labelled point in the aforementioned figures. Table 4 summarizes the conditions associated with each of the points.

The effect of secondary flow on the baseline ejector performance is shown in Fig. 16. The data were obtained using the air inbleed venturis at various steam driving pressures and different diffuser exit pressures. The figure presents the data as the ratio of cell pressure to minimum (no secondary flow) cell pressure versus secondary to primary mass flow ratio. The data indicate that for a secondary flow ratio of 0.04, the cell pressure for the started diffuser has increased by approximately 40 percent, and at a secondary flow ratio of 0.13, the cell pressure is doubled. The data in the figure contain approximately 20 percent scatter. Observations of fluctuations in cell pressure readings on the control room display indicated that the flow inside the test cell was unsteady. The discrete measurement of unsteady flow conditions could be the source of the scatter shown in Fig. 16.

4.1.2 Rocket Tests

Three rocket tests were conducted with the baseline configuration. The first test evaluated system operation with the steam ejector started and operating at low levels of steam and backpressure. The second test was conducted with an unstarted ejector at high steam and backpressures. The last of the baseline configuration rocket tests was conducted with a started ejector at a high steam pressure and moderate backpressure.

Figure 17 shows the results of the first rocket test. The exit pressure, P_{ex}, was set at 2.0 psia and the steam pressure, P_{tst}, was held constant at 63 psia. The steam ejector was initially started with a normalized exit pressure of 0.032. The motor burn was nominally 2.4 sec long with a maximum chamber pressure just below 2,000 psia. After ignition, the test cell pressure, P_{cell}, immediately dropped, then followed the contour of the rocket motor chamber pressure trace (i.e., P_{cell}/P_{tc} is constant). This indicates that the rocket diffuser was started. The rocket diffuser unstarted when the rocket motor chamber pressure decreased during motor tailoff. The chamber pressure value at diffuser unstart was too low to be measured reliably. The ejector diffuser backpressure, P_{ex}, varied during the motor firing. The transition duct volume just downstream of the ejector diffuser exit (see Fig. 3) was pumped down by the combined steam-rocket exhaust flow. As the rocket chamber pressure tailed off, the backpressure increased as seen in Fig. 17.

The second rocket test evaluated operation with higher steam and exit pressures and an initially unstarted diffuser. The results are shown in Fig. 18. The exit and steam driving pressures were 8.0 and 190 psia, respectively. The baseline steam-only data showed that this condition was insufficient to start the ejector prior to ignition. As a result, the cell pressure prior to ignition was substantially higher than would have been encountered if the ejector was started. After ignition, the rocket diffuser started and pumped the cell down to approximately 0.5 psia. The rocket diffuser unstarted at 22 percent of maximum chamber pressure.

The last rocket test of the baseline configuration evaluated operation at a high steam driving pressure and a backpressure reduced to permit started operation of the ejector prior to ignition. The results are presented in Fig. 19. Since the ejector was started, the cell pressure at ignition was substantially lower than the previous case, 0.6 versus 2.5 psia, respectively. Upon ignition, the rocket diffuser again started and pumped the cell down to near 0.2 psia. The rocket diffuser unstarted at 14 percent of maximum chamber pressure. The rocket diffuser unstarted at a higher chamber pressure than the first case due to the higher rocket diffuser backpressure as caused by the higher steam driving pressure.

The rocket diffuser started and operated for three different steam ejector operating conditions. Therefore, there is no indication that the steam ejector is incompatible with the tested rocket motor/diffuser combination.

4.2 EFFECT OF THROAT LOCATION

4.2.1 Steam Tests

The effect of diffuser second throat location relative to the ejector nozzles was evaluated by testing alternate Configurations 2, 3, 4, and 5, listed in Table 1. The results of these tests, summarized in Table 3, were compared to the baseline results.

The breakdown curve for the baseline and alternate throat location configurations is shown in Fig. 20. The data indicate that as the throat is moved forward, the cell pressure decreases slightly until the throat is located at the nozzle exit plane. At this location, there is a strong degradation in cell pressure. The normalized exit pressure at which breakdown occurs does not vary significantly. The effect of throat location on maximum diffuser pressure rise is shown in Fig. 21. The rise ratio increases slightly as the throat is moved forward from 4/3 to 1/3 diffuser diameters because of the decrease in cell pressure. The correspondence of rise ratio to throat location over this region is nearly linear. However, when the throat is located at the nozzle exit plane there is a significant decrease in rise ratio.

Based on Bauer and German's previous experimental work with central ejectors (Ref. 3), there is a limit on the distance of the second throat contraction from the nozzle exit beyond which it is not possible to start the diffuser. This type of limit was not encountered in the current research. However, this does not imply that such a limit does not exist. The central nozzle tests showed a limit on the order of 4 diameters. This is far outside the range of locations investigated in this study. It should also be noted that the central nozzle tests used air for the primary gas. It is not known what effect the nozzle geometry and gas composition have on the limiting value of throat location.

The wall pressure measurements from the nozzle exit plane through the throat ramp are shown in Fig. 22 for the five throat location configurations. The wall pressure measurement at the nozzle exit plane was measured on the rearward facing step below the nozzle in what is expected to be a recirculation zone for the flow. Configuration 2, with the throat inlet located at the nozzle exit, had increased wall pressures below the nozzle exit and at the first measurement station on the ramp. The other configurations show a trend of decreased wall pressure with distance, except for the case with the throat located farthest downstream, where there is a strong pressure rise on the throat ramp that is not present for the other configurations.

4.2.2 Rocket Tests

Two rocket firings were conducted with the ejector diffuser second throat located 4/3 diameters downstream of the ejector nozzle exit plane (Configuration 5). One firing was conducted at the low steam and backpressures, and one firing was conducted at a higher steam pressure. Both tests were conducted in such a manner that the steam ejector was started.

The results of the low steam pressure test are shown in Fig. 23. As evidenced by the test cell pressure data, the rocket diffuser started and remained started throughout the firing. As with the baseline configuration rocket test at the same conditions, the rocket chamber pressure at diffuser unstart was too low to be measured reliably. The high steam pressure test results are presented in Fig. 24. In this case,the rocket diffuser started and remained started until 17 percent of maximum chamber pressure. The increase in cell pressure noted at approximately 0.8 sec is believed to be caused by rocket exhaust gas leaking into the test cell from a crack in the graphite nozzle insert. This crack was discovered during posttest examination of the motor. Such a crack would degrade the rocket thrust; therefore, the stream thrust at diffuser unstart may have actually been closer to the baseline configuration result than the chamber pressure data indicate.

One motor firing was conducted with the ejector diffuser second throat positioned 2/3 diameter downstream of the ejector nozzle exit plane (Configuration 5). This firing was conducted with a high steam pressure and an initially started diffuser. The results of this

test, shown in Fig. 25, indicate that the rocket diffuser started and remained started until the motor chamber pressure decreased to 15 percent of its maximum value. Note also that the cell pressure exhibits an increase during the motor firing similar to that seen in Fig. 24. Again, posttest inspection revealed a crack in the graphite nozzle insert.

4.3 EFFECT OF THROAT CONTRACTION

4.3.1 Steam Tests

The effect of throat contraction was evaluated by comparing the results from the baseline and Configuration 6, both of which are shown Table 3. The breakdown curve for both configurations is shown in Fig. 26. The data indicate that as the throat diameter is decreased, the maximum exit pressure at breakdown increases, as expected from central nozzle tests (Ref. 3). The data also indicate an increase in cell pressure. However, this increase may be attributable to a slight test cell air inleakage. The effect of throat contraction on maximum diffuser pressure rise is shown in Fig. 27. For the two configurations evaluated, the trend is increased rise ratio for decreased area ratio.

In a manner similar to the throat location problem, Jones (Ref. 6) indicated that there is a limit on the second throat area ratio, A_{st}/A_d, below which the ejector will not start. Both tested ejectors started; thus, the geometries did not exceed the limiting value. Based on the diffuser inlet Mach number, Jones' limit curve suggests a limiting contraction ratio of approximately 50 percent for the current ejector, which is well below the configurations tested. However, Jones experimentally defined the limit curve for centerbody ejectors flowing gaseous nitrogen and, therefore, it may not be accurate for the annular steam ejector.

Wall pressure measurements for the two throat contractions are shown in Fig. 28. Two sets of four data points, taken at similar conditions, are shown for both diffuser configurations. At the overdriven (steam pressure well above the level required for starting) and underdriven (steam pressure below the level required for starting) conditions, the curves for the two configurations are similar. However, for the intermediate curve, the smaller throat shows a slightly steeper average pressure recovery gradient than the baseline.

4.3.2 Rocket Tests

Two rocket firings were conducted with an ejector diffuser second throat contraction of 0.7 (Configuration 6). Firings were conducted at the low and high steam pressures, nominally the same conditions tested with the baseline and Configuration 5.

The results of the low steam pressure test are shown in Fig. 29. The rocket diffuser started and remained started throughout the firing. The results of the high steam pressure test are

presented in Fig. 30. These data indicate that the rocket diffuser started and remained started until 18 percent of maximum chamber pressure. This level is higher than was recorded for the baseline, possibly because of the the smaller throat; however, the increase is so small that it may only be attributable to the uncertainty of the data.

4.4 EFFECT OF RAMP ANGLE

4.4.1 Steam Tests

The effect of second throat ramp angle was examined by comparing the results from the baseline and Configuration 7, shown in Table 3. The breakdown curve for both configurations is shown in Fig. 31. The data indicate that as the ramp angle is increased there is a slight degradation in the cell pressure. As with the effect of contraction ratio, some of this increase may be attributable to the presence of secondary flow from inleakage. Essentially no change is seen in the maximum normalized exit pressure. The increase in cell pressure reduces the overall rise ratio as shown in Fig. 32. As can be seen from the figure, the effect of ramp angle on rise ratio is not very strong. Further, the actual effect may be weaker if the data are corrected for the cell inleakage for the Configuration 7 test.

Bauer and German data (Ref. 3) for centerbody ejectors agree with the current data in that the effect of ramp angle is very small. Regardless, the purpose for testing Configuration 7 was to verify that the ramp angle did not have a large effect for annular ejectors.

The wall pressure measurements for the two diffusers are shown in Fig. 33. The two sets of data points were taken at similar operating conditions and show little difference in the wall pressure profiles. Since there were no significant overall system differences at the steeper ramp angle, no major differences were expected in the wall profiles.

4.4.2 Rocket Tests

One motor firing was conducted with the ejector diffuser second throat ramp angle increased from 5 to 6.5 deg (Configuration 7). This firing was conducted with a high steam pressure and a started diffuser. The results of this test, shown in Fig. 34, indicate that the rocket diffuser started and remained started until chamber pressure decreased to 20 percent of its maximum value. This is 6 percent higher than the baseline. The measured increase might be attributed to the increased effective blockage of the steam plume. The steam is entering the diffuser at a steeper angle but at the same initial momentum as the baseline. As a result, the steam penetrates farther into the rocket exhaust stream. However, it must be remembered that the increase relative to the baseline is the same order of magnitude as the uncertainty, so the actual change, if any, attributed to physics cannot be accurately quantified.

5.0 APPLICATION OF COMPUTATIONAL TECHNIQUES TO EJECTOR PERFORMANCE PREDICTION

An effort was made to determine if a typical current computational fluid dynamics (CFD) code could be applied to an ejector configuration to predict major aspects of the flow. This process is referred to as CFD program calibration based on the definitions given by Bradley (Ref. 15), as reported by Garrard and Phares (Ref. 16). If the calibration was successful, the program would then be applied to the subscale test configuration reported in the previous sections to verify the ability of the program to model the critical physics of the flow accurately. As per Bradley, this second step is referred to as program validation. Upon successful validation, the program could be applied to other ejector designs to investigate parametric effects.

The PARC code (Ref. 16) was selected for application because it has been used extensively and lends itself well to problems involving multiple stream mixing and complex geometries. The PARC code is a general-purpose CFD program that provides aerodynamic flow-field simulation using the Reynolds-averaged Navier-Stokes equations for a single phase, single species ideal gas. The study used Version 5.0 of the code which is the latest version documented in the reference.

The code calibration effort was begun before the experimental data were taken; therefore, an alternate data set was required. The existing Hale and Gobbell data (Ref. 9) for a second throat annular ejector were utilized. The geometry for this case, Configuration 11a in Fig. 11, was considered to be sufficiently similar to the baseline configuration to provide a basis for code calibration. Because the geometry was axisymmetric, the 2-dimensional/axisymmetric version of the PARC code was used.

A comparison of computed to measured cell pressure as a function of nozzle total and diffuser exit pressures was selected as the primary metric for evaluating code performance. The PARC code was to be calibrated by computing the flow field for the specified geometry at a set nozzle total pressure and diffuser exit pressure. Then the numerical values for the coefficient of turbulent mixing in the algebraic turbulence model would be adjusted until the computed and measured cell pressure matched. Upon successful completion of this step, the code would be evaluated by computing solutions for other nozzle total and diffuser exit pressures and comparing the results to the experimental breakdown curve.

The calibration was initiated by modelling the second throat geometry, shown in Fig. 11, and applying boundary conditions such that P_{ex}/P_{tst} had a value of 0.03. The code also required a specification of the ratio of specific heats for the gas. A value of 1.3 was input for the specific heat ratio. The initial solution for the cell pressure is shown in Fig. 35, labelled

γ = 1.3 (PARC), along with the experimental data. The code prediction of cell pressure was too low by a factor of 3.

Next, the coefficient of turbulent mixing was varied in an attempt to match the cell pressure to the data. However, for the current ejector, variation of the coefficient had virtually no effect on the cell pressure. Because the same process of manipulating the viscous effects had been successfully performed by Garrard and Phares (Ref. 16), other aspects of the code were called into question for this application.

It was hypothesized that for the ejector flow field, condensation effects are more significant than viscous effects. Because the PARC code does not have a mechanism to model the physics of condensation, the use of the PARC as a stand-alone code was discarded and a new computational methodology was formulated.

The new approach was to account for condensation in the steam ejector nozzle first and then, using these new nozzle exit conditions, compute the diffuser flow field with PARC, neglecting the condensed water phase. Condensation effects in the ejector nozzle were assessed using FIRACON (Ref. 17), a NASA Langley code for one-dimensional finite-rate water condensation. This code was adapted and applied to the steam nozzle ejector problem. The new nozzle exit conditions included a higher static pressure and a ratio of specific heats of 1.19. Cell pressure was predicted using the PARC code with the steam nozzle exit plane fixed to the gas property values computed by FIRACON. Results of this computation are shown in Fig. 35 and are labelled "γ = 1.19 (FIRACON/PARC)." While this approach was an improvement, the computed cell pressure was still low by 30 percent.

The sensitivity of the diffuser flow field to γ was further investigated through a variation of γ from 1.19 to 1.08 to account for condensation beyond the nozzle exit (with the latter γ value chosen arbitrarily). These results are also shown in Fig. 35. In this case, the computed cell pressure was high by approximately 10 percent. At this point the calibration effort was terminated. Theoretically, the code could have been 'calibrated' by varying γ until the cell pressures matched. However,changing a flow field γ to account for condensation within the flow field does not represent the physics of the flow accurately. The PARC code would still be unable to account for the change in the gas mass flow rate as the steam condenses, and it is the mass flow balance of gas entrainment and recirculation that determines cell pressure.

The calibration effort concluded that the PARC code (as used) was insufficient to predict ejector flows. A phase change model and a two-phase conservation equation need to be incorporated into PARC before the code can be successfully calibrated. At that point, an effort can be made to validate the code for a specific geometry.

6.0 SUMMARY OF RESULTS

A baseline configuration second throat annular steam ejector was tested with steam only, steam with inbleed air, and combined steam and rocket exhaust flows. Six alternate configurations were tested in addition to the baseline design to investigate the effects of geometric variables on the baseline design.

1. The baseline ejector started and operated with a maximum pressure ratio across the system of 12.

2. Test cell atmospheric inbleeds had a strong effect on the cell pressure. A secondary flow of 4 percent of the steam flow increased cell pressure by 40 percent.

3. The rocket diffuser started for the baseline and all alternate configurations tested with rocket exhaust flows.

4. Second throat location affected operation by decreasing the cell pressure, and therefore increasing the pressure rise, as the throat was moved forward from the baseline design. When the throat was moved to the plane of the ejector nozzle exit, the cell pressure increased significantly. There was no discernable effect on rocket diffuser unstart.

5. A smaller contraction ratio second throat diffuser increased the maximum exit pressure, and, therefore, pressure rise, of the system. The contraction ratio effect on rocket diffuser unstart pressure was smaller than the measurement uncertainty.

6. Variation of the ramp angle did not have a significant effect on the ejector operating characteristics. A small increase in the rocket diffuser unstart pressure was observed.

7. The computational study indicates that condensation effects appear to be much more significant than viscous effects in the diffuser/ejector flow field.

8. Use of version 5.0 of the PARC code as a stand-alone predictive tool is inadequate for ejector flows because it is limited to single-phase flow with an ideal gas equation of state.

7.0 RECOMMENDATIONS

1. Additional geometries should be tested to determine the starting limits for throat location and throat contraction for second throat annular ejectors.

2. Tests should be conducted to determine the interaction effects between variables, e.g., comparing the results of a test with a smaller throat moved forward versus the separate results reported herein for the size and movement effects.

3. The PARC code should be modified to include the ability to model two-phase steam flow with finite-rate nucleation and condensation.

REFERENCES

1. Porter, J. L. and Squyers, R. A. "A Summary/Overview of Ejector Augmentor Theory and Performance." ATC-R-91100/9CRL-47A, Vought Corporation Advanced Technology Center, September 1979.

2. Lewis, G. E. and Drabble, J. S. "Ejector Experiments." NGTE R-151, National Gas Turbine Establishment, February 1954.

3. Bauer, R. C. and German, R. C. "The Effect of Second Throat Geometry on the Performance of Ejectors without Induced Flow." AEDC-TN-61-133, Arnold Engineering Development Center, November 1961.

4. Panesci, J. H. and German, R. C. "An Analysis of Second Throat Diffuser Performance for Zero-Secondary-Flow Ejector Systems." AEDC-TDR-63-249, Arnold Engineering Development Center, December 1963.

5. German, R. C. and Panesci, J. H. "Improved Methods for Determining Second-Throat Diffuser Performance of Zero-Secondary-Flow Ejector Systems." AEDC-TR-65-124, Arnold Engineering Development Center, July 1965.

6. Jones, W. L., Price, H. G., and Lorenzo, C. F. "Experimental Study of Zero-Flow Ejectors Using Gaseous Nitrogen." NASA TN D-203, March 1960.

7. Hickman, K. E., Hill, P. G., and Gilbert, G. B. "Analysis and Testing of High Entrainment Single-Nozzle Jet Pumps with Variable-Area Mixing Tubes." NASA-CR-2067, June 1972.

8. Johnston, S. C. "Experimental Investigation of a Supersonic Air Air Ejector Operating with a Second Throat." von Karman Institute for Fluid Dynamics, VKI TN 45, August 1968.

9. Hale, J. W. and Gobbell, W. C. "Diffuser Auxilliary Ejector Development for the Design of the J-3 LEM Descent Exhaust System." AEDC-TR-65-255, Arnold Engineering Development Center, February 1966.

10. Haroldsen, O. O. "Ejector Model Test Program for J-2 Altitude System." R-5699, North American Rockwell Corp., Rocketdyne Division, May 1964.

11. Addy, A. L. "On the Steady State and Transient Operating Characteristics of Long Cylindrical Shroud Supersonic Ejectors." Ph.D. Dissertation, Department of Mechanical Engineering, University of Illinois, 1963.

12. Owens, C. L. "Calibration Capabilities of ETF Instrument Branch." AEDC-TR-67-18 (AD648707), March 1967.

13. Thompson, J. W. and Abernathy, R. B., et al. "Handbook of Uncertainty in Gas Turbine Measurements." AEDC-TR-73-5 (AD755356), February 1973.

14. Taylor, D. "Ejector Designs for a Variety of Applications." AGARDOGRAPH 163, November 1972, pp. 103 - 164.

15. Bradley, R. G. "CFD Validation Philosophy." Paper No. 1., AGARD Symposium on Validation of Computational Fluid Dynamics, May 1988, Lisbon, Portugal.

16. Garrard, G. D. and Phares, W. J. "Calibaration of the PARC Program for Propulsion-Type Flows." AEDC-TR-90-7, July 1990.

17. Erickson, Wayne D., et al. "Finite-Rate Water Condensation in Combustion-Heated Wind Tunnels." NASA Technical Paper 2833, 1988.

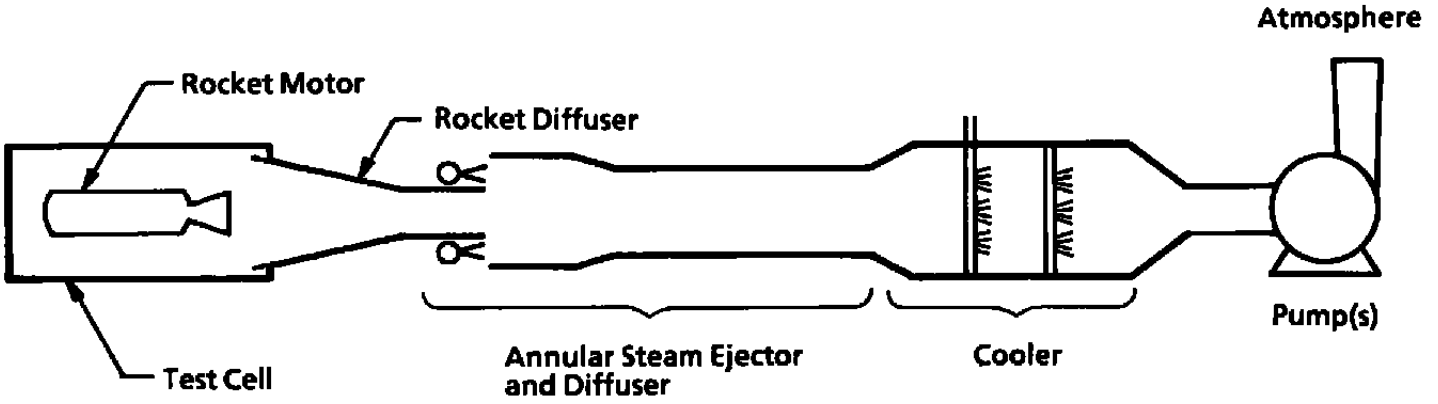

Figure 1. Rocket motor altitude test facility.

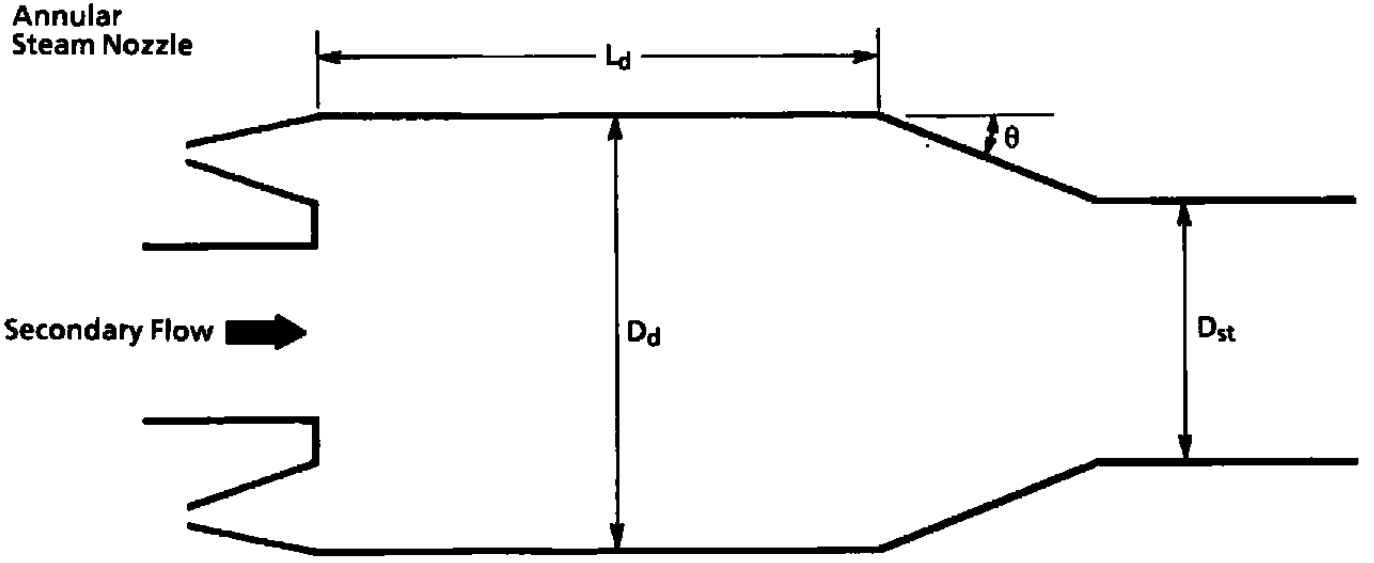

Figure 2. Second throat annular steam ejector.

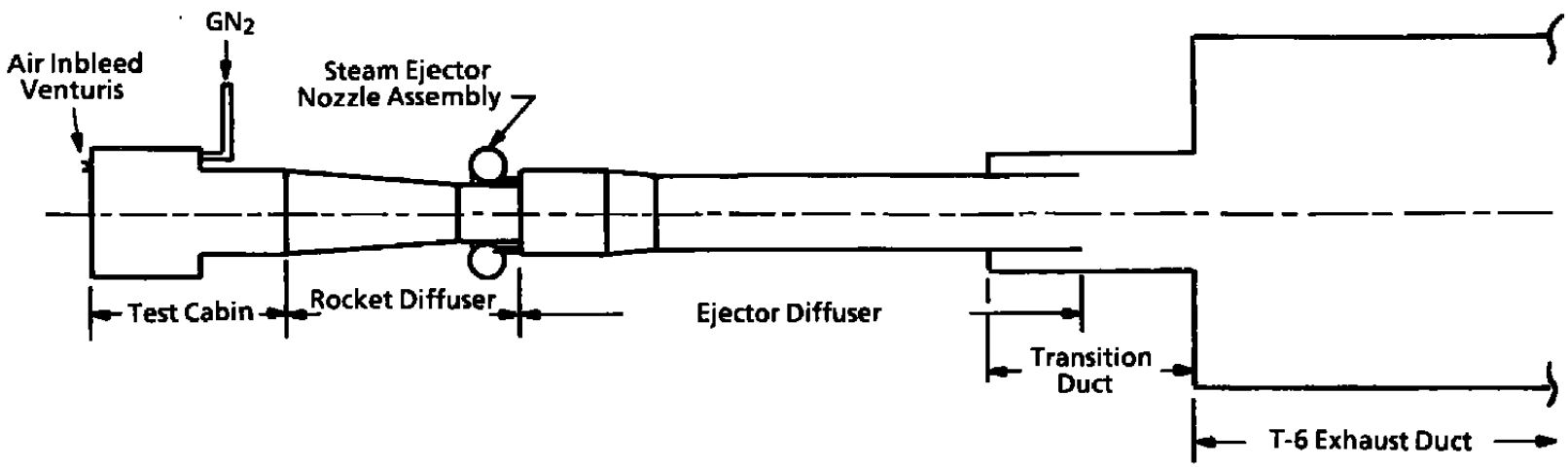

Figure 3. Test configuration.

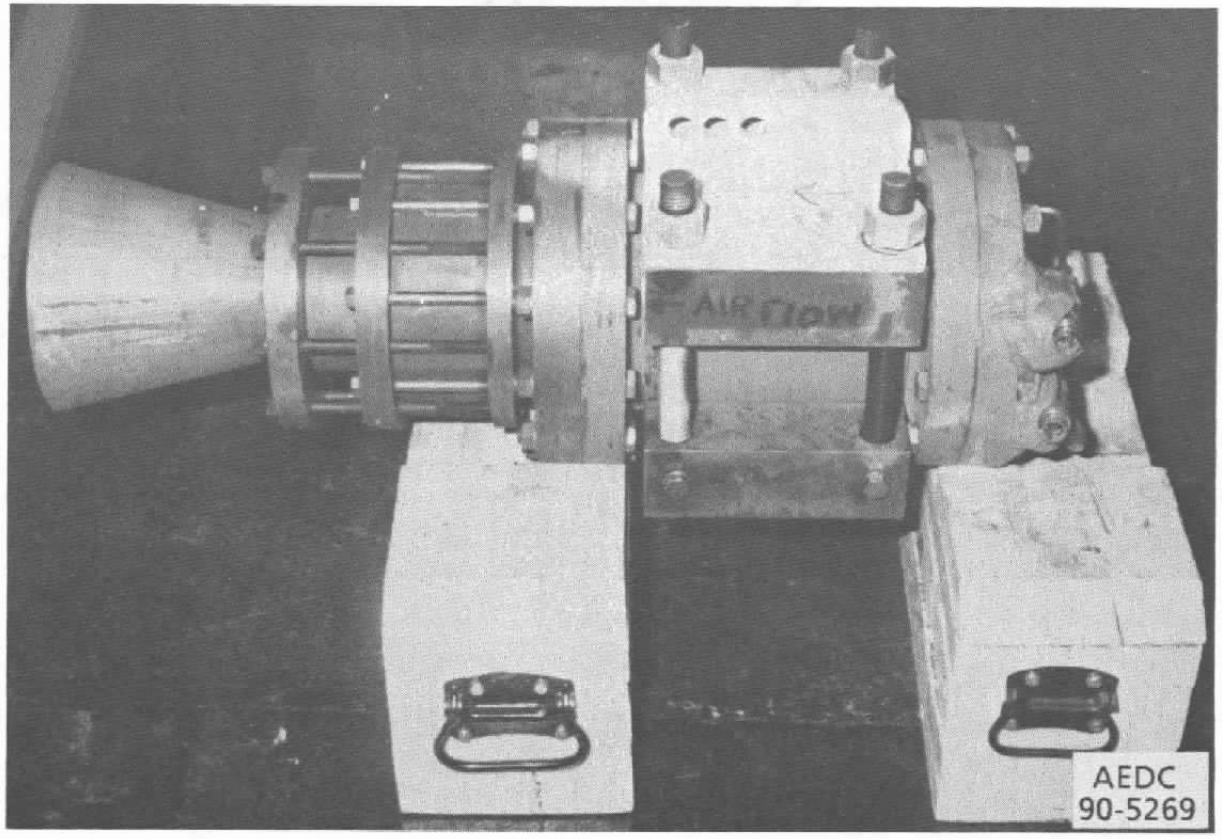

a. Photograph

Figure 4. BATES solid-propellant rocket motor.

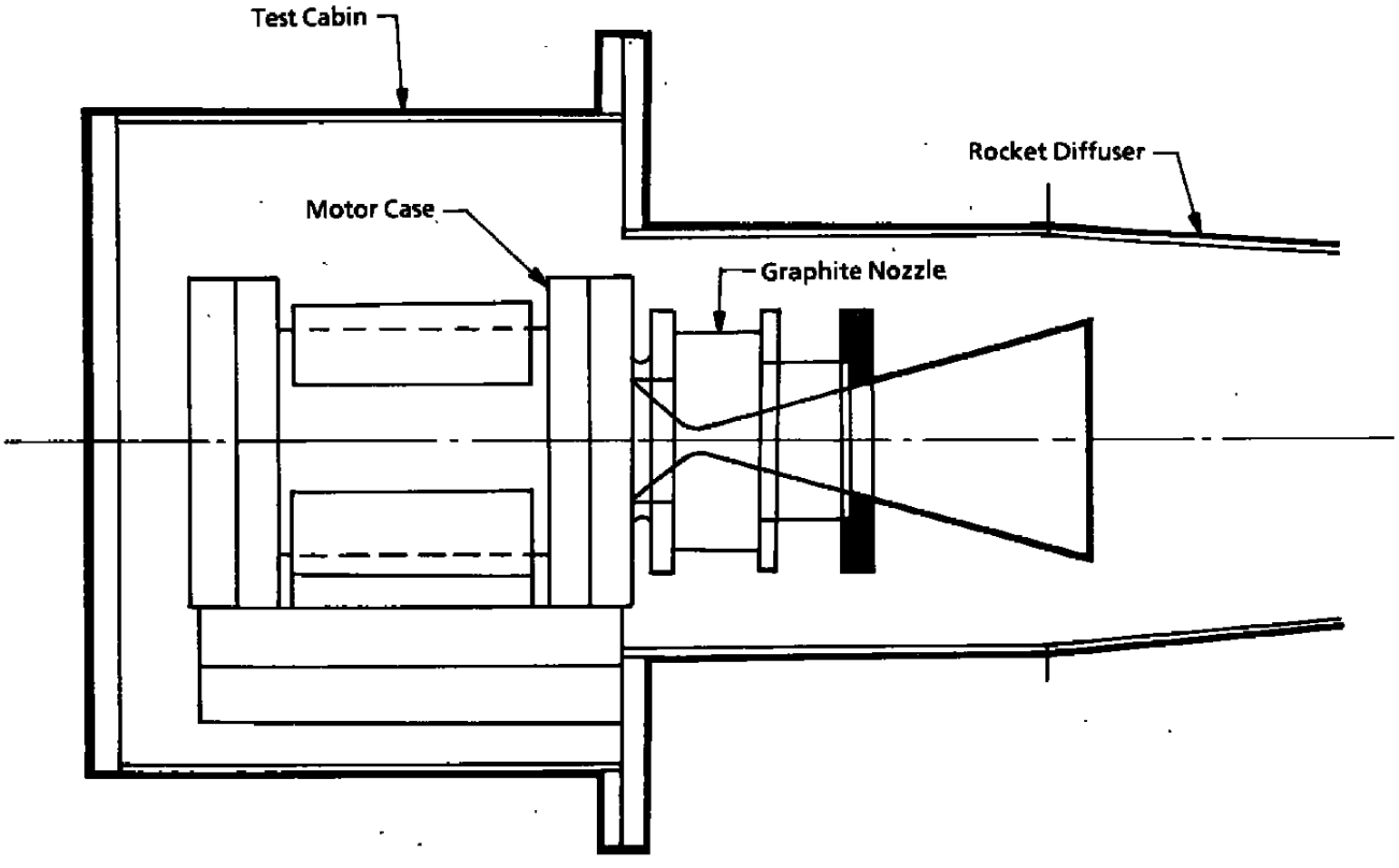

b. Motor installed in test cell
Figure 4. Concluded.

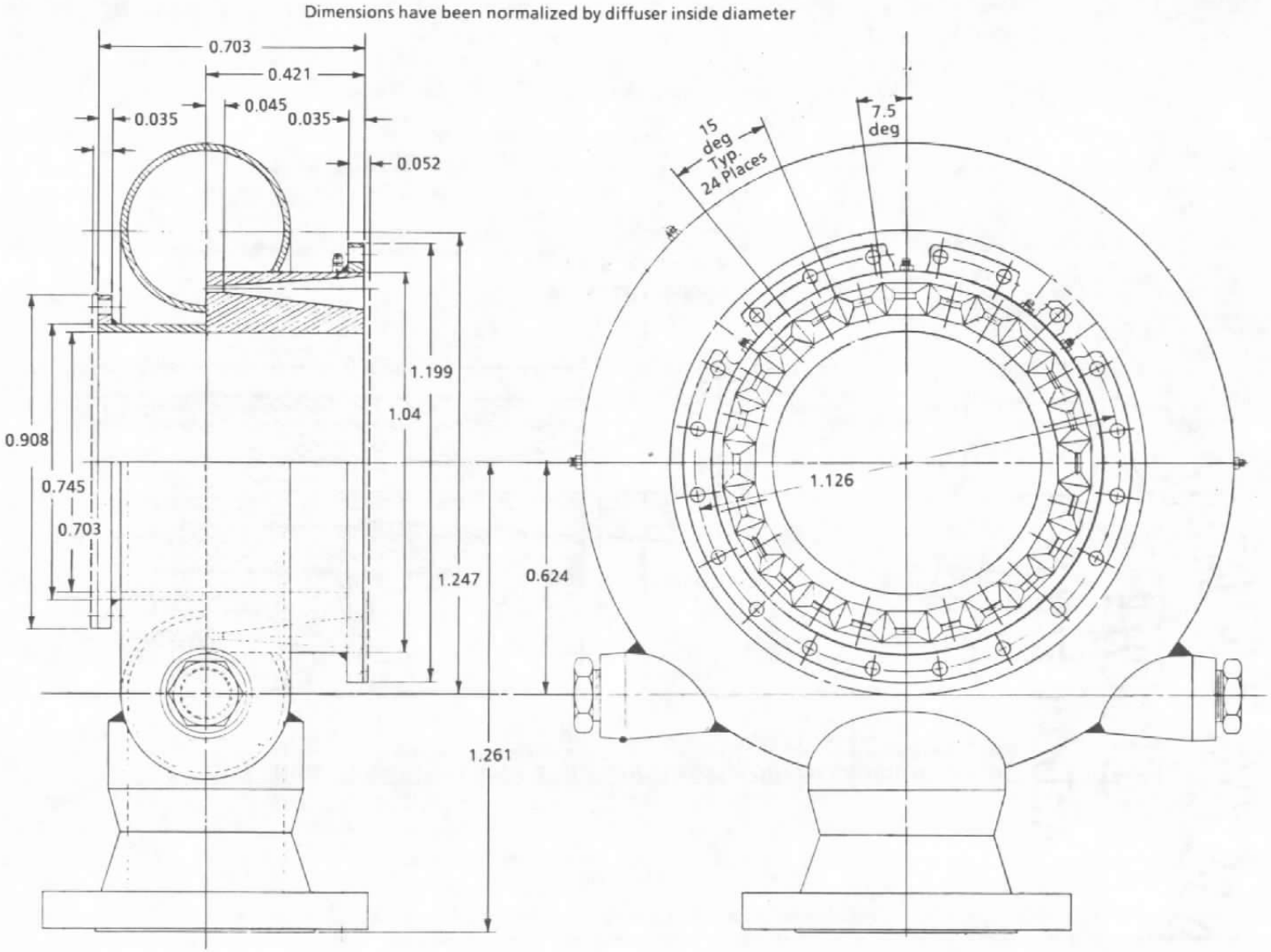

a. Manifold/nozzle assembly

Figure 5. Steam ejector geometry.

Note: Dimensions have been normalized by diffuser inside diameter.

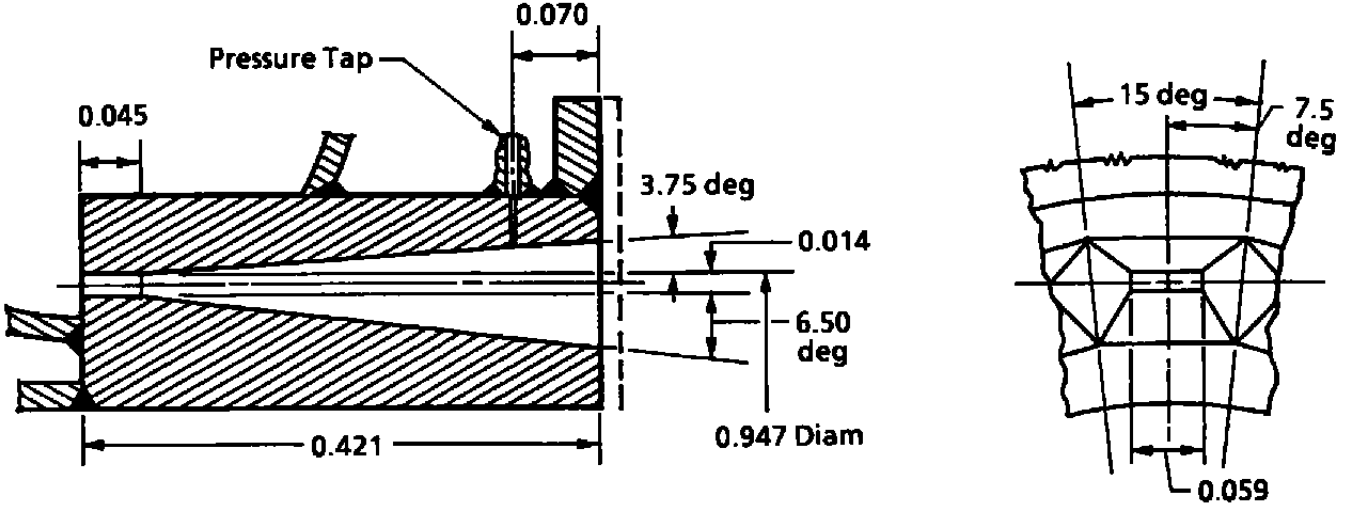

b. Nozzle details
Figure 5. Concluded.

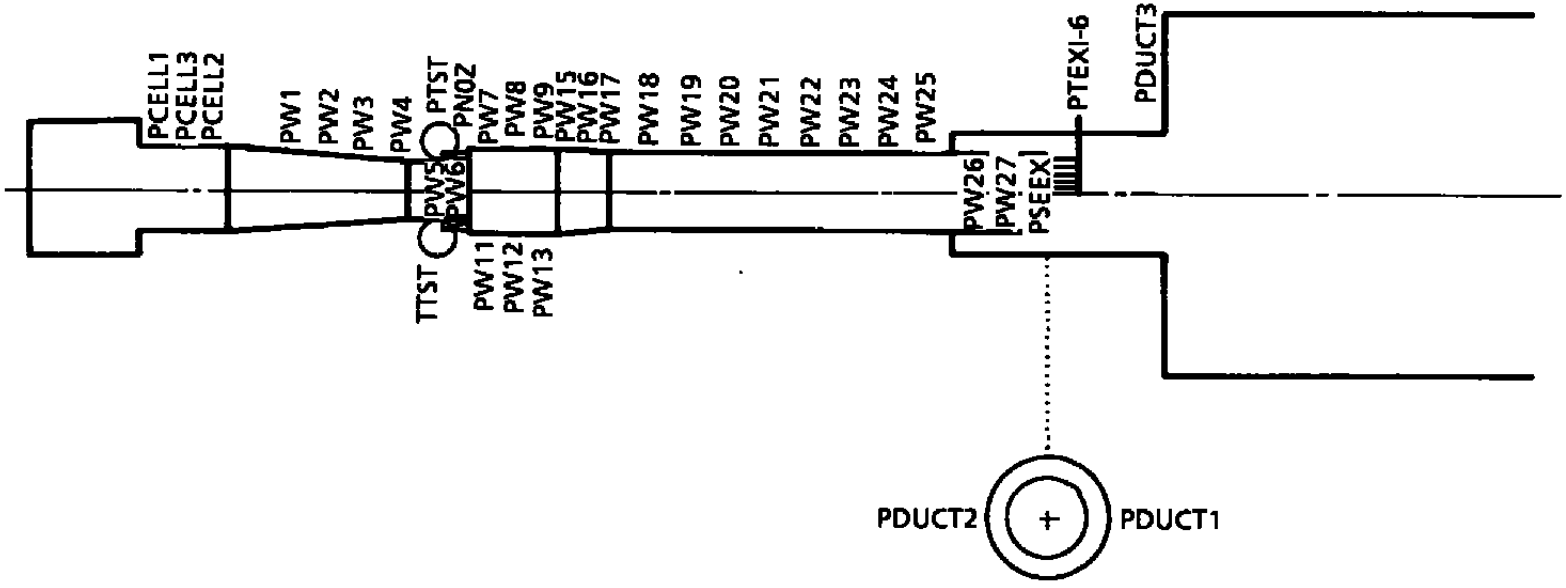

Figure 6. Test instrumentation locations.

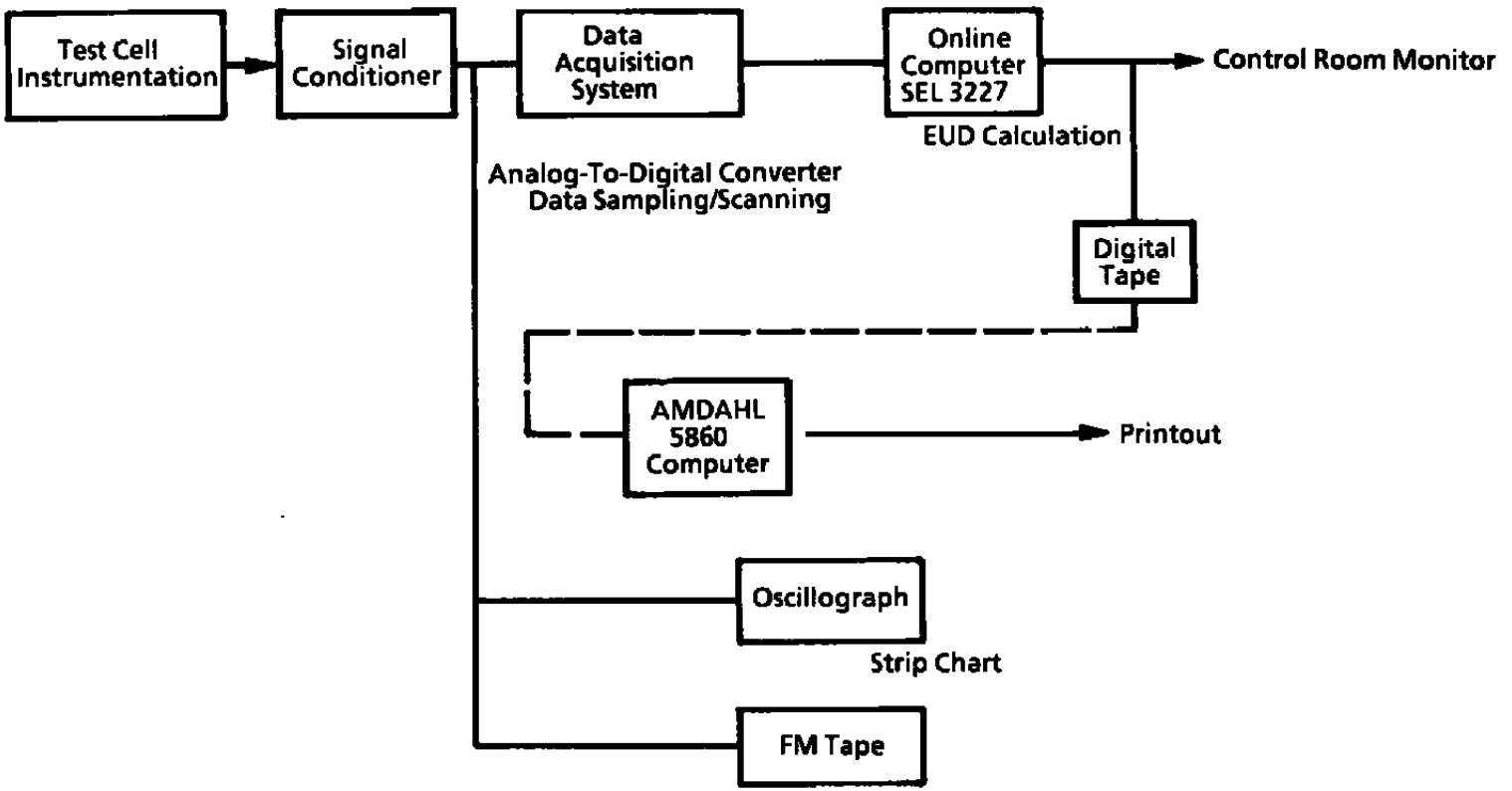

Figure 7. Instrumentation system schematic.

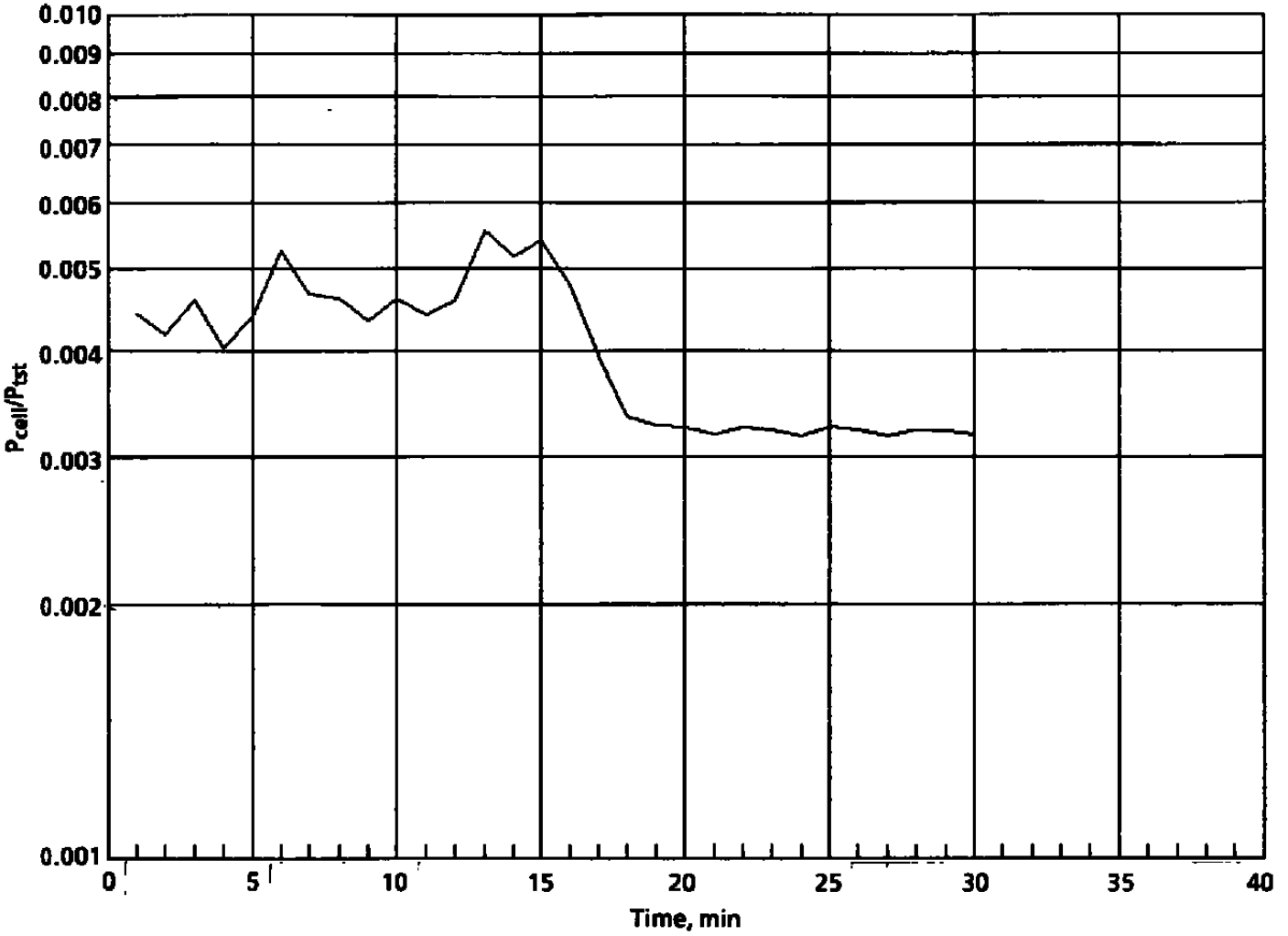

Figure 8. Typical time trace for steam system stabilization.

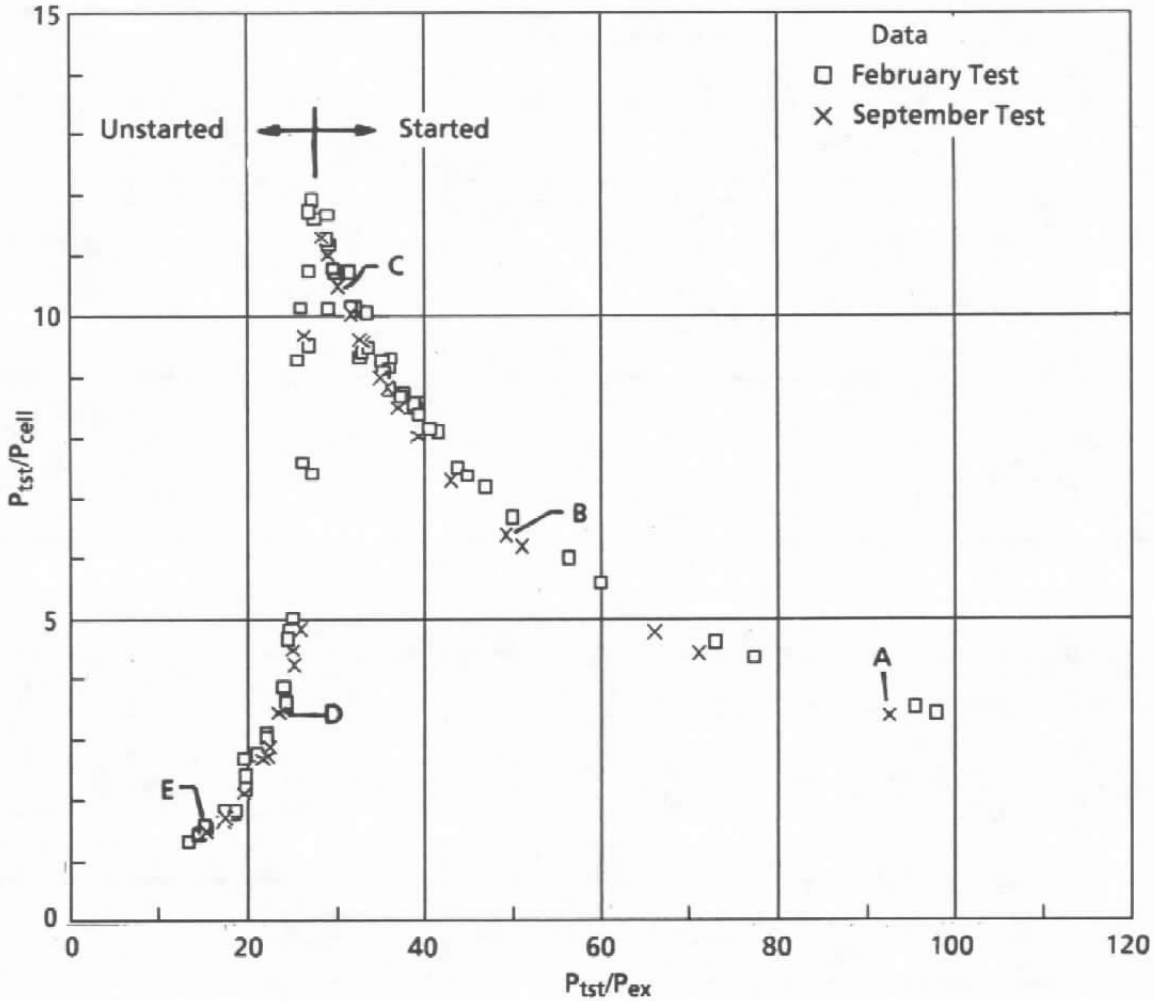

Figure 9. Steam ejector rise ratio versus normalized total pressure for baseline design.

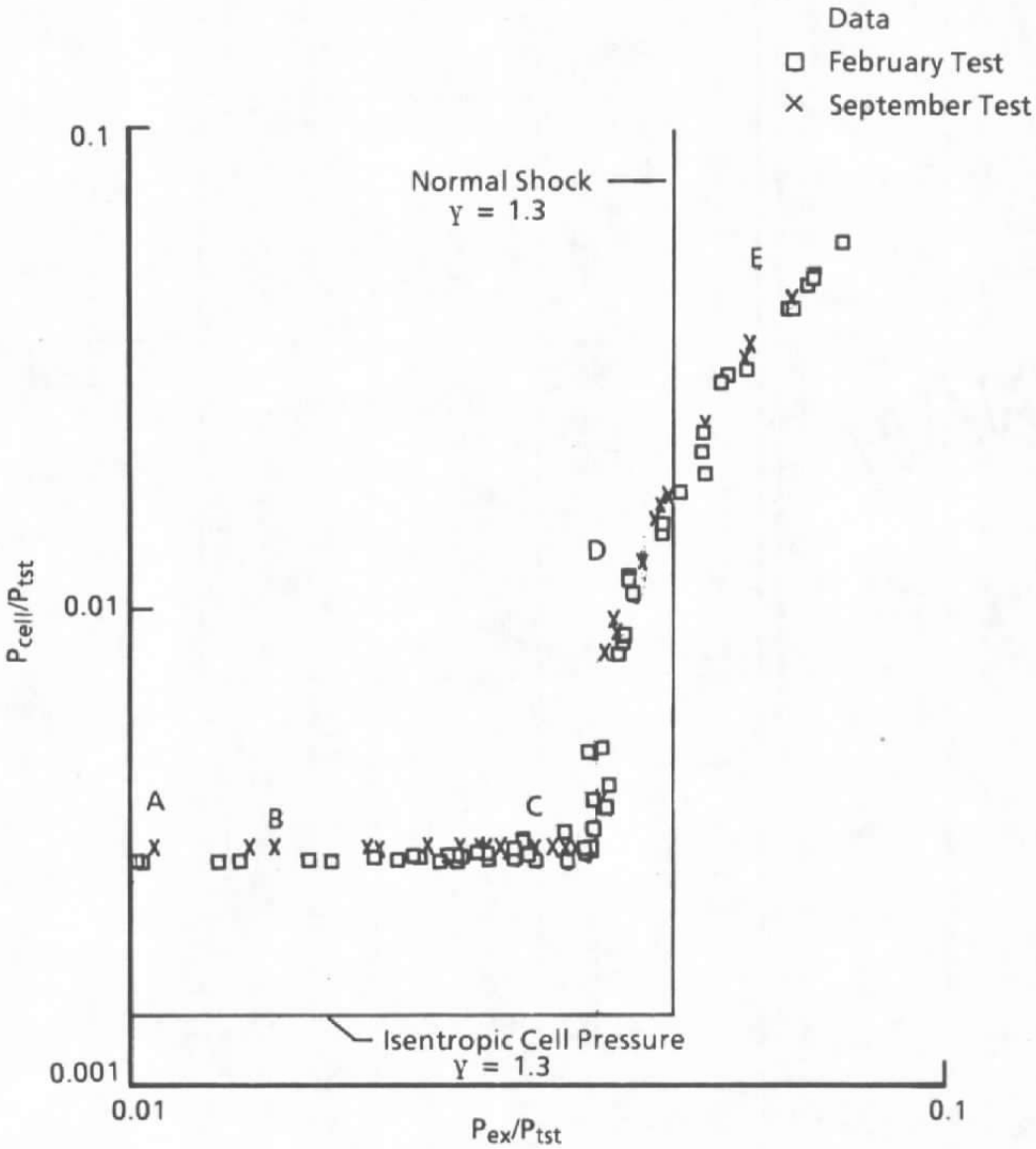

Figure 10. Steam ejector breakdown curve for baseline design.

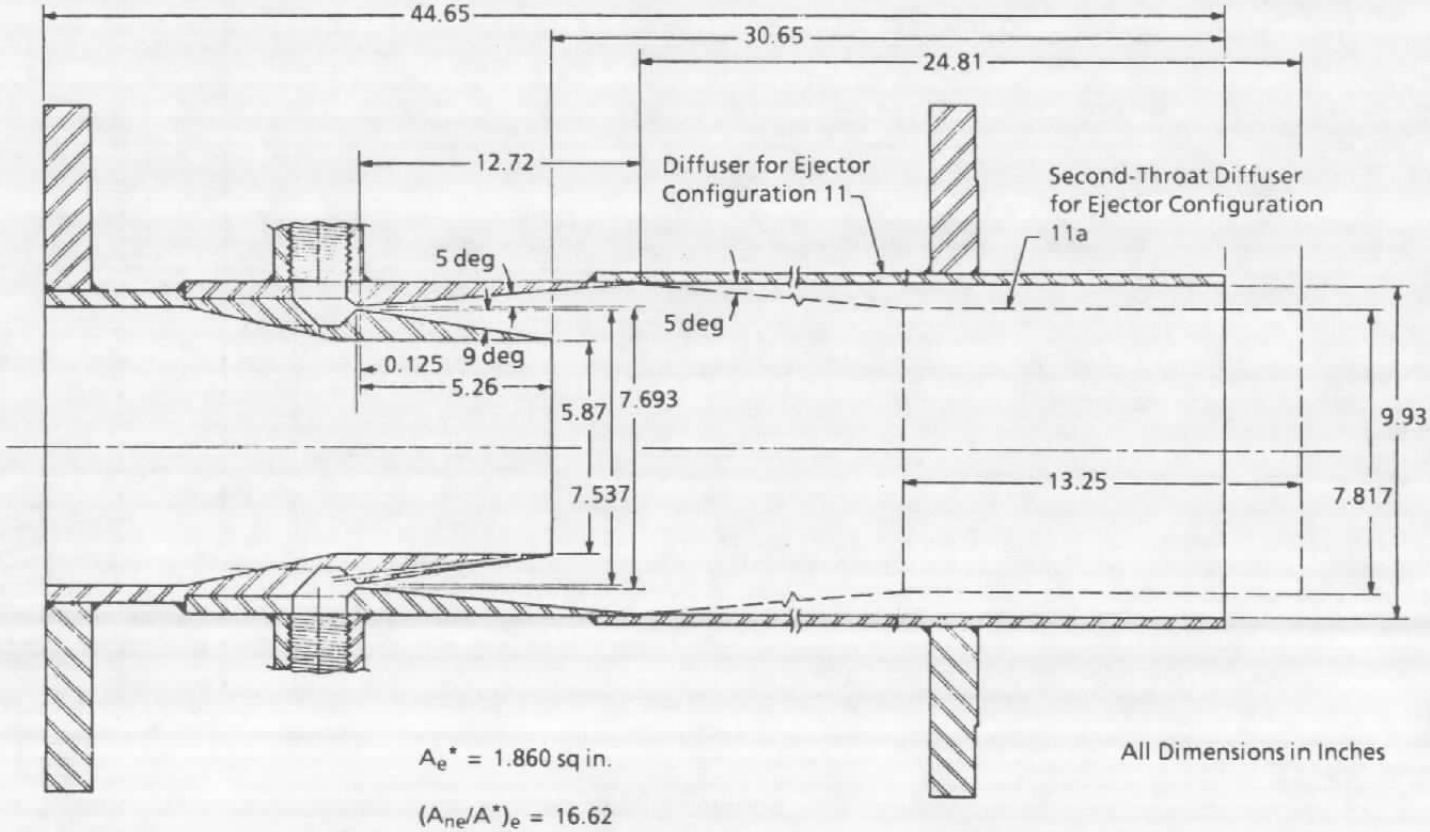

Figure 11. Hale and Gobbell's annular ejector configurations (Ref. 9).

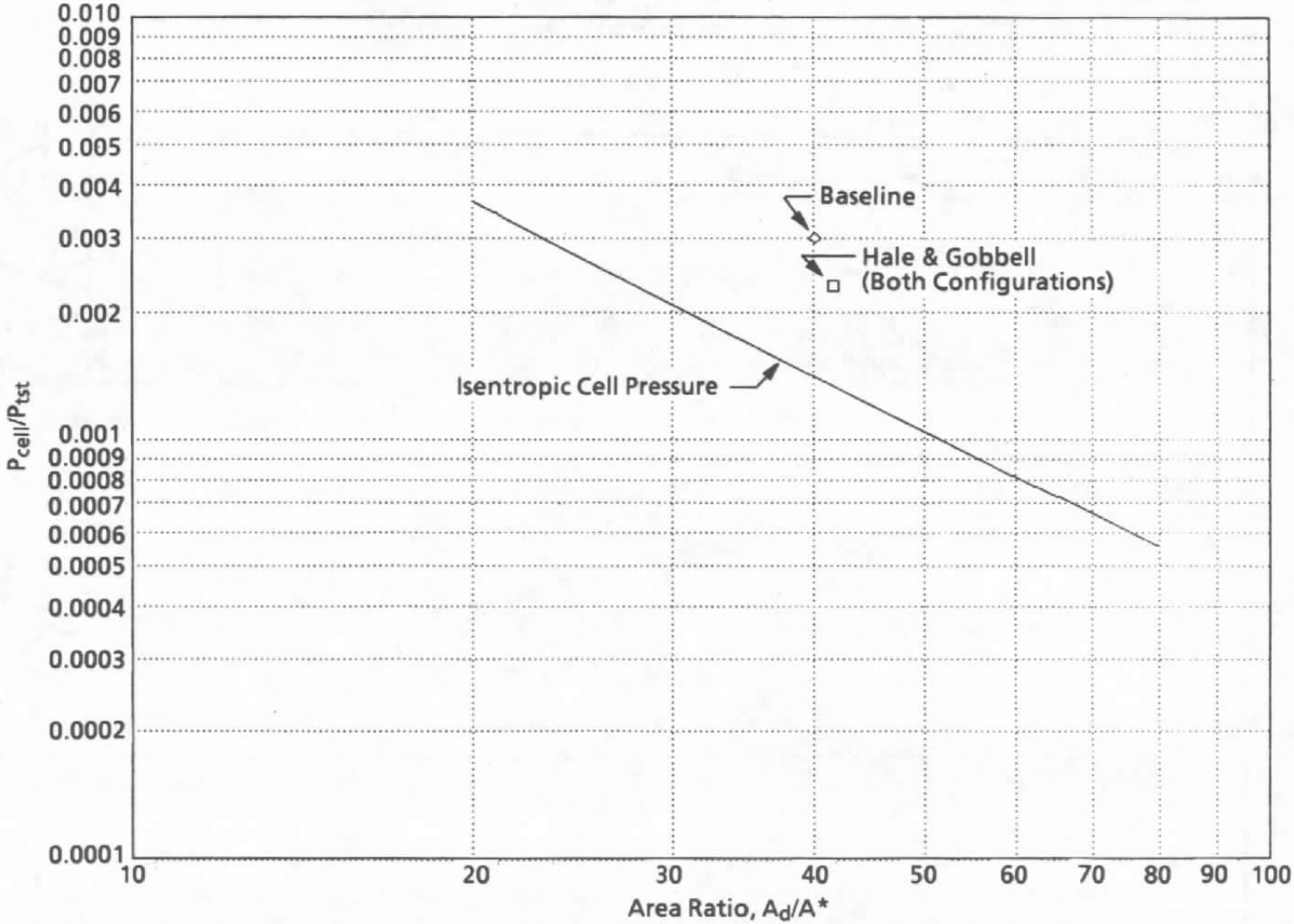

a. Minimum cell pressure

Figure 12. Comparison of baseline to data of Hale and Gobbell (Ref. 9).

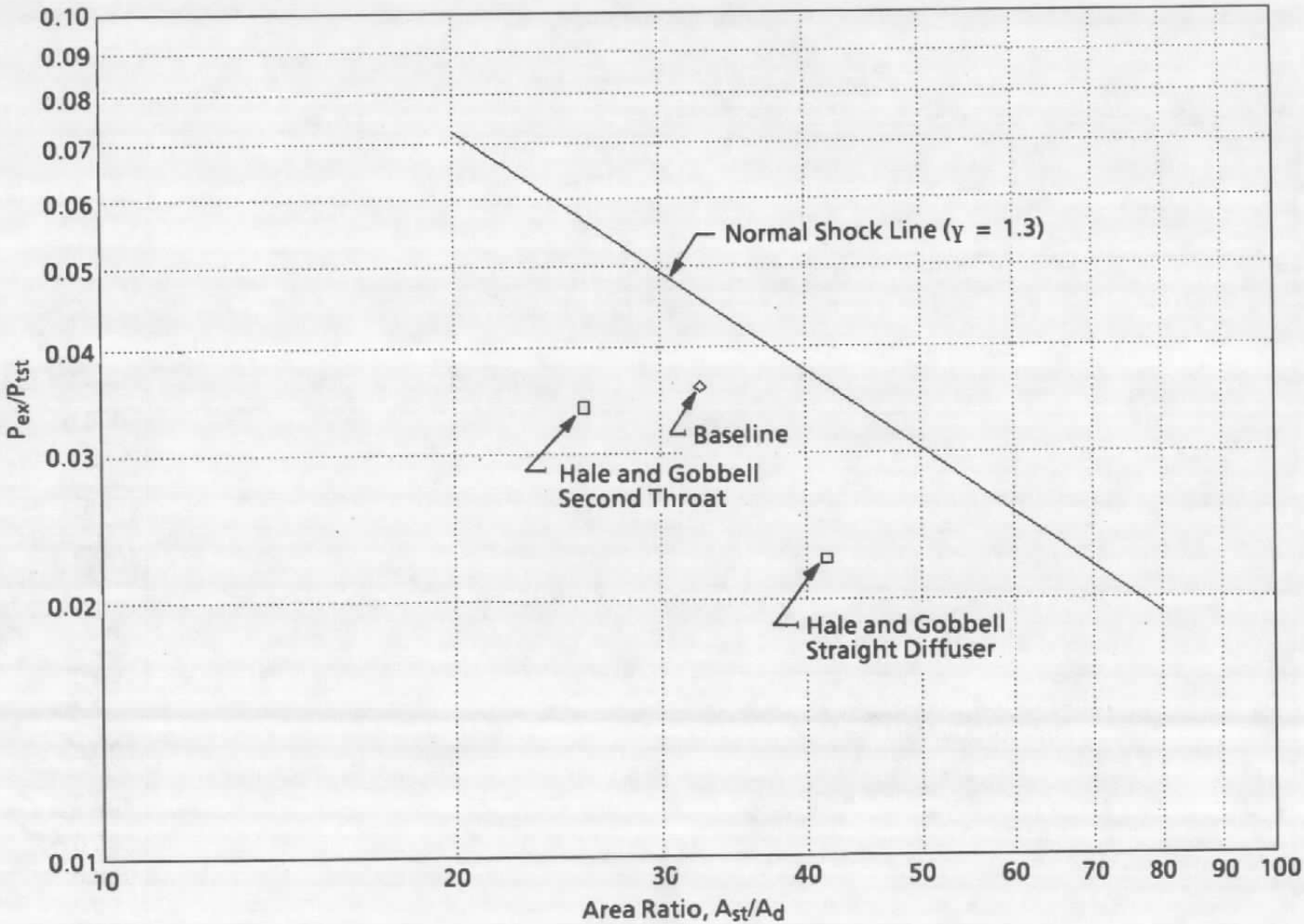

b. Exit pressure

Figure 12. Concluded.

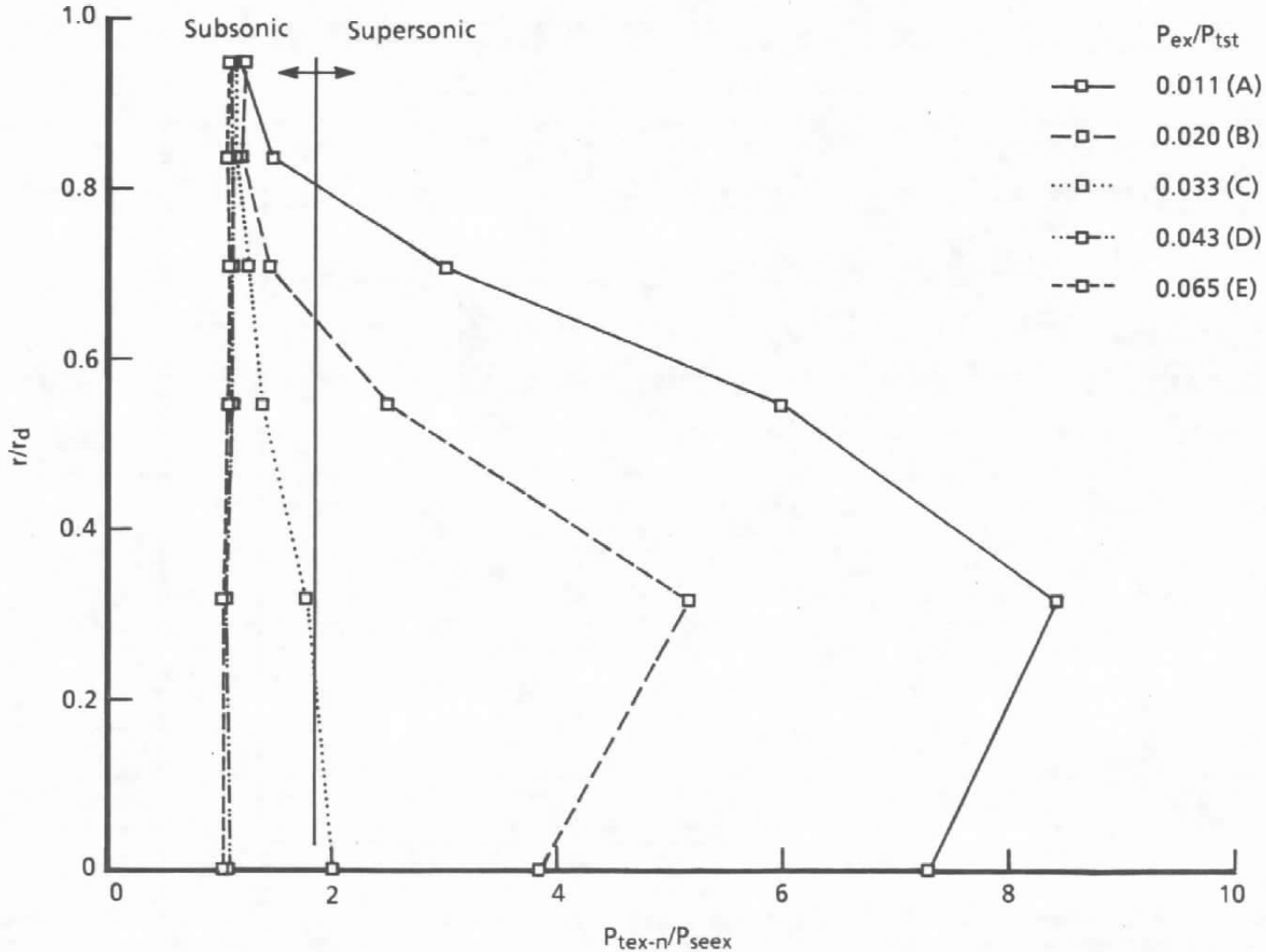

Figure 13. Ejector diffuser exit pitot pressure profiles.

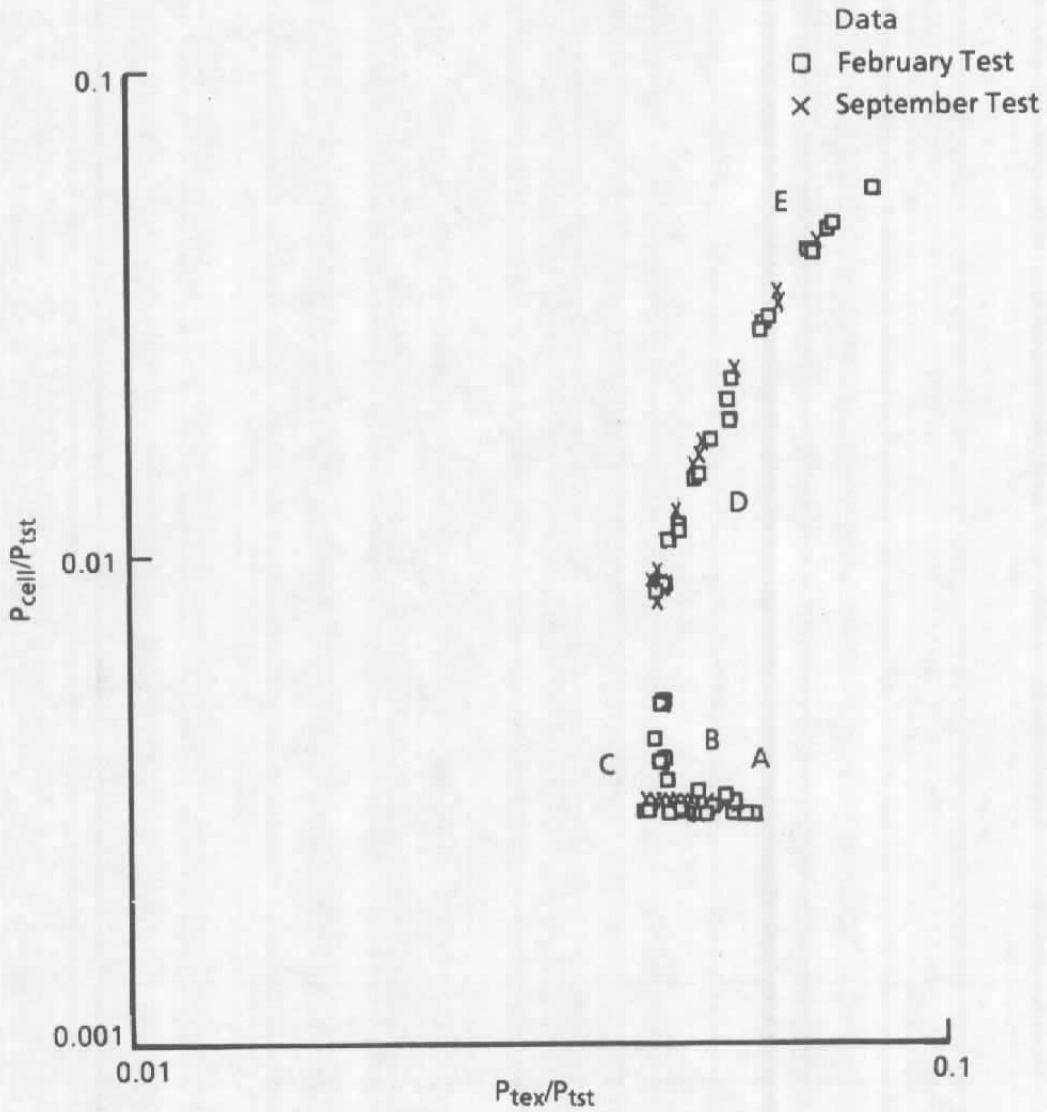

Figure 14. Normalized cell pressure versus rake average exit pitot pressure.

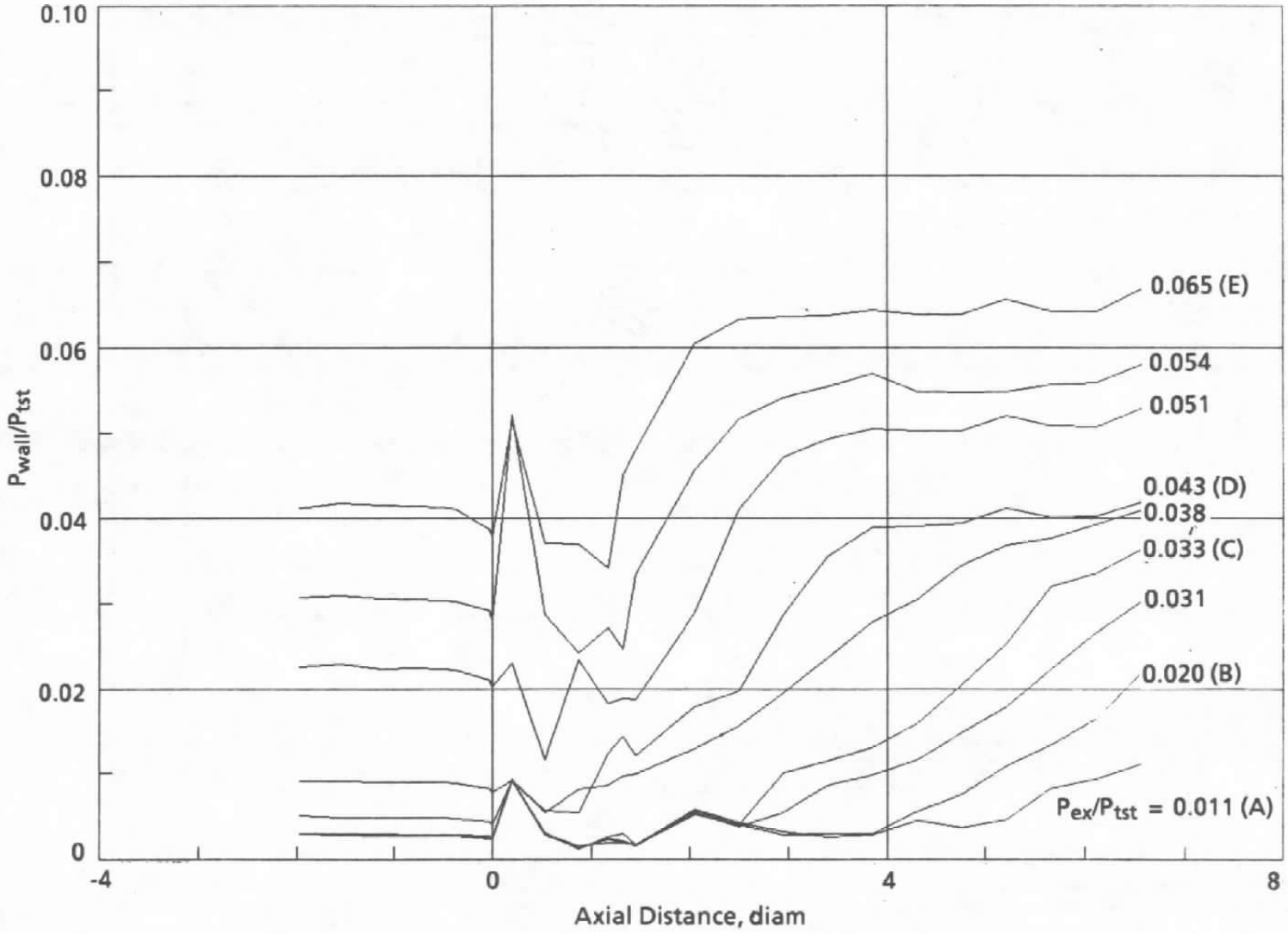

Figure 15. Baseline wall pressure profiles.

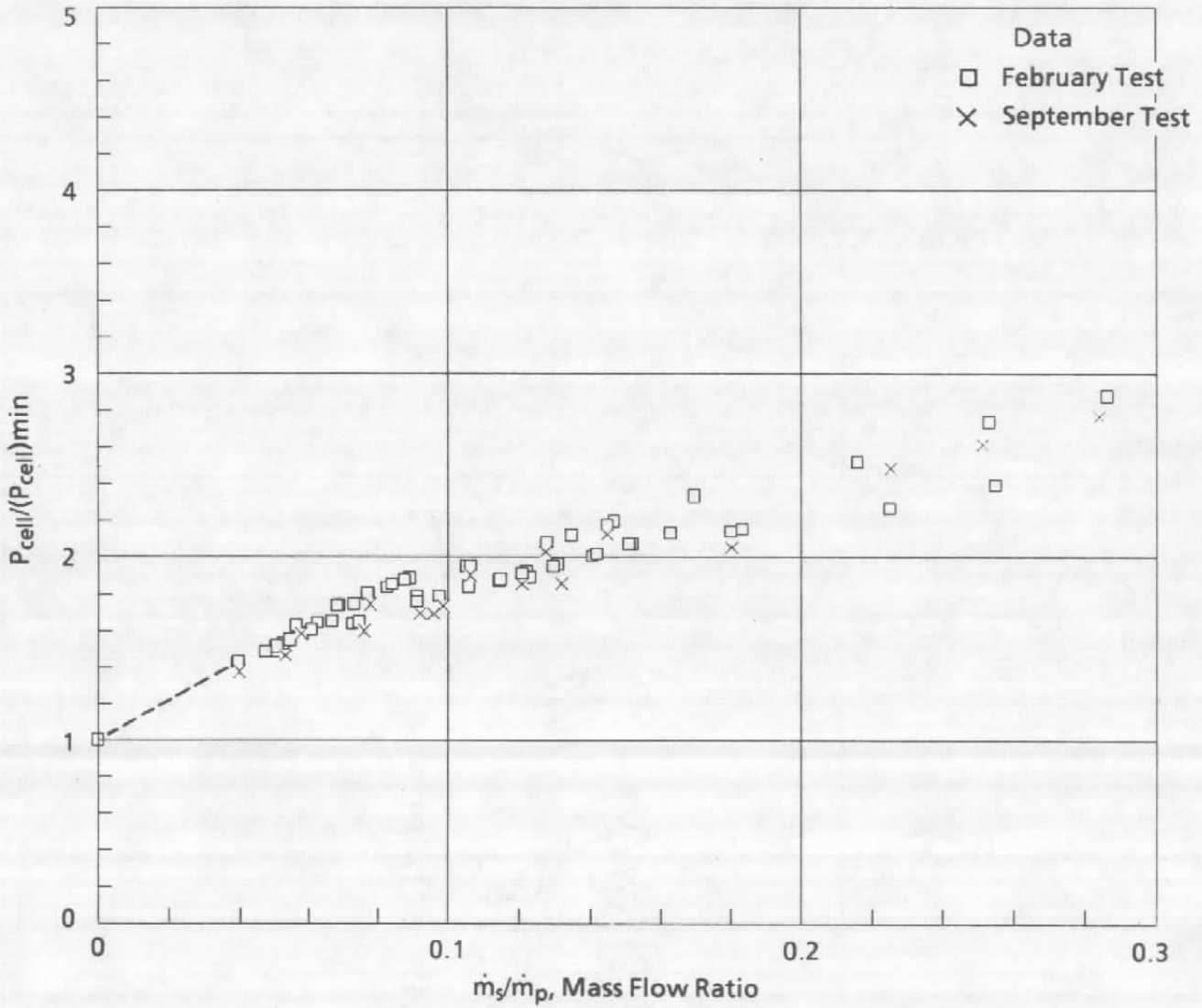

Figure 16. Effect of secondary flow on miminum cell pressure.

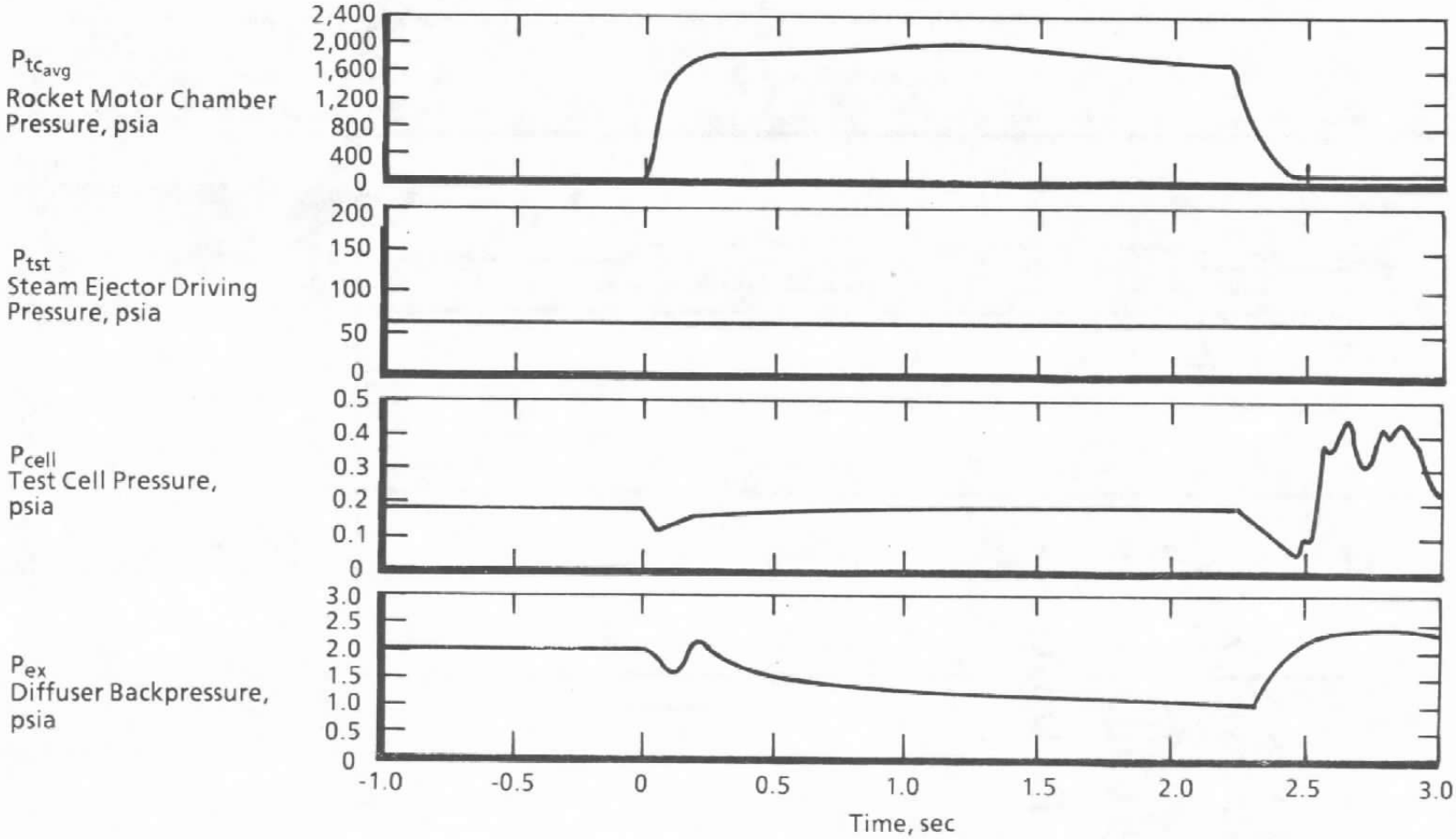

Figure 17. Rocket test results for baseline at low steam and exit pressures—started diffuser

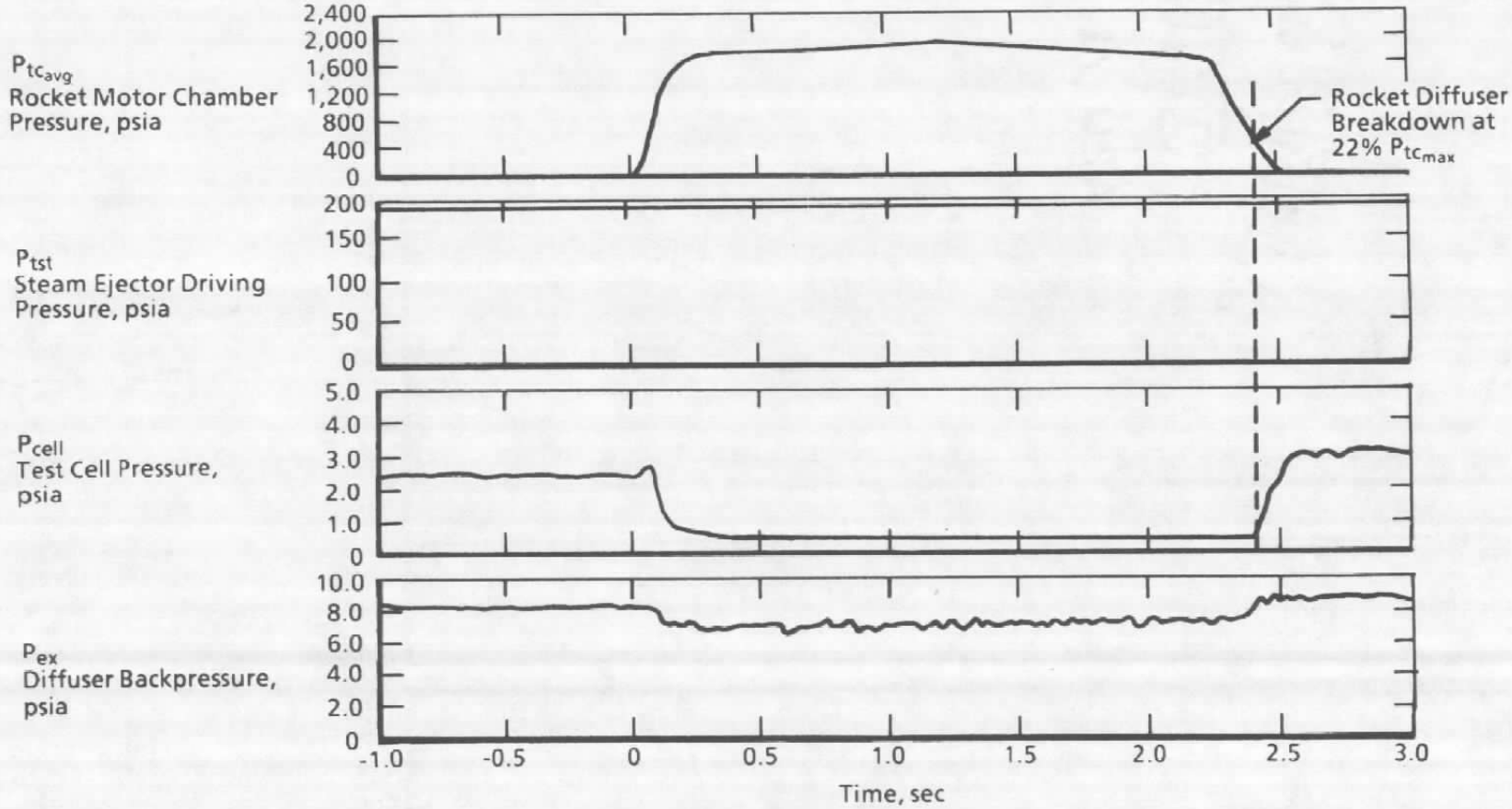

Figure 18. Rocket test results for baseline at high steam and exit pressures—unstarted diffuser.

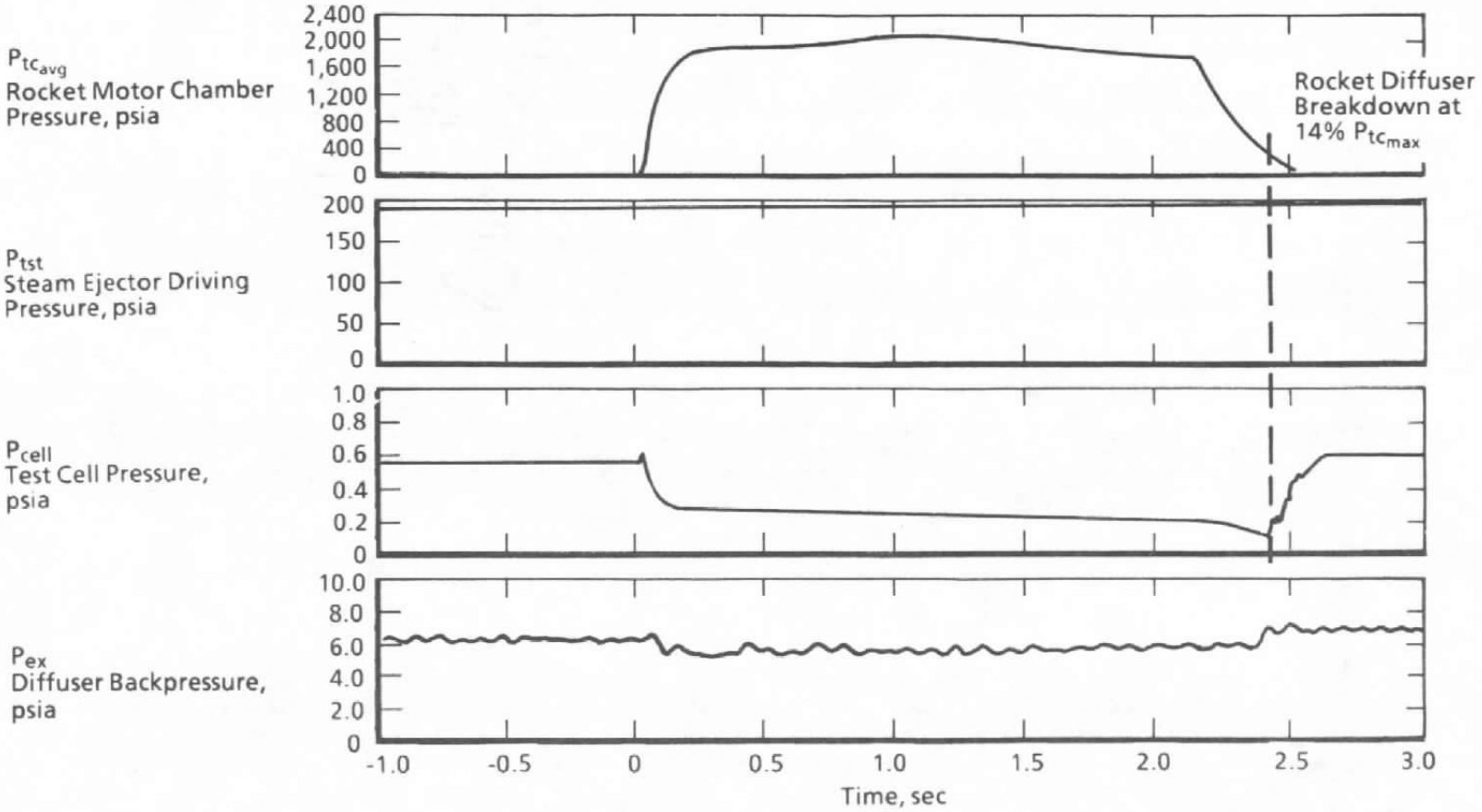

Figure 19. Rocket test results for baseline at high steam pressure and started diffuser.

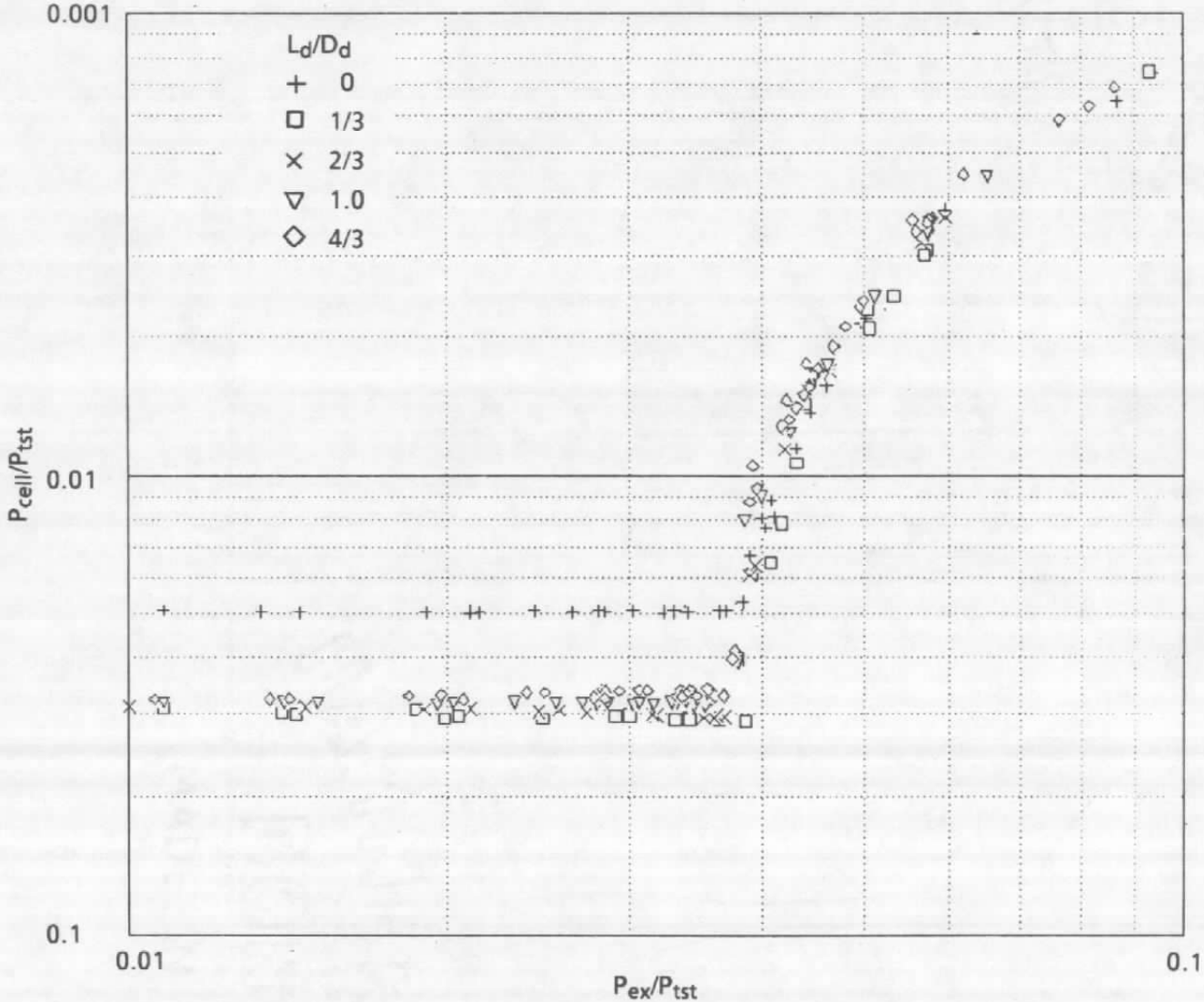

Figure 20. Effect of throat location on ejector breakdown curve.

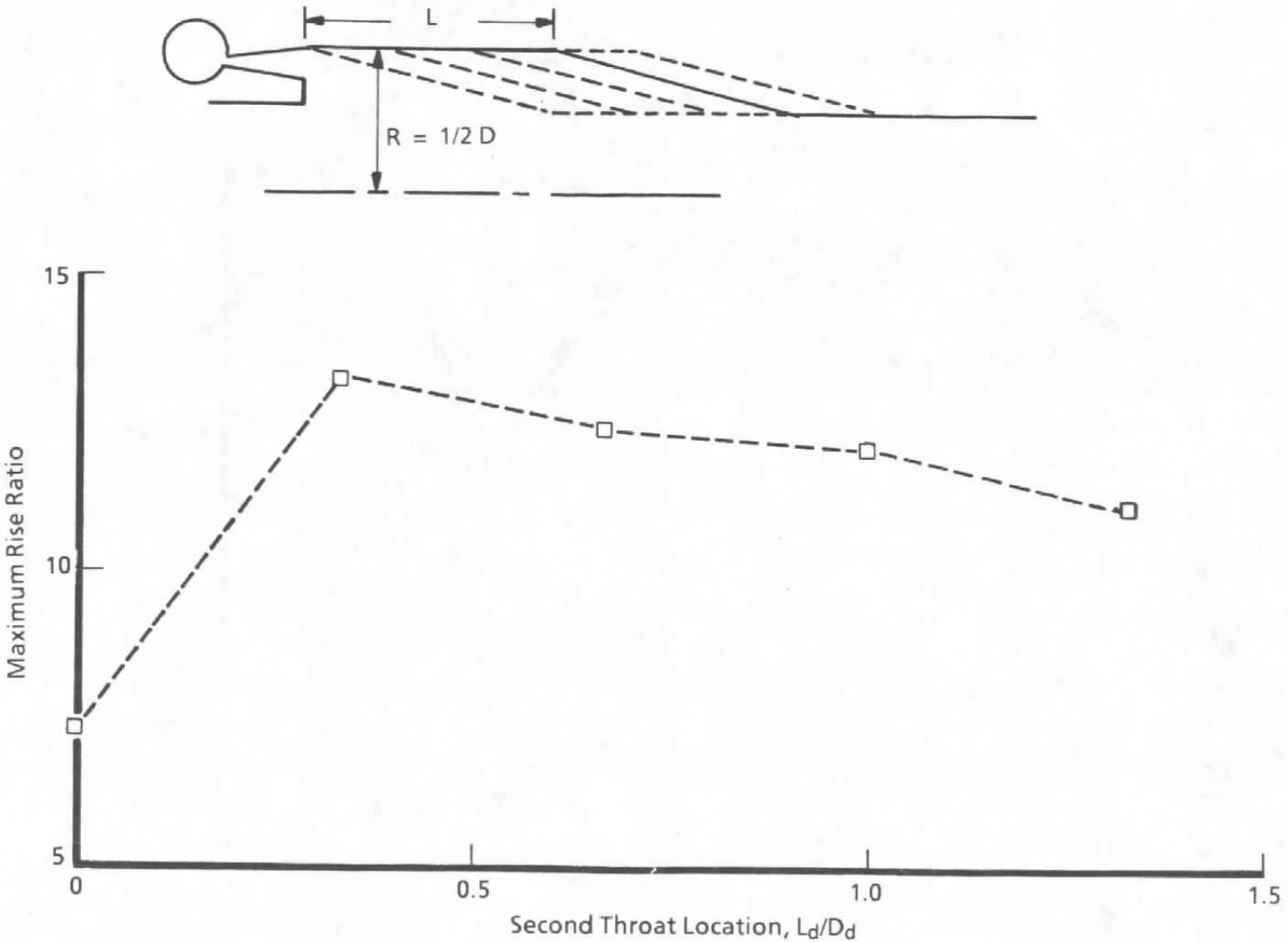

Figure 21. Effect of throat location on maximum rise ratio.

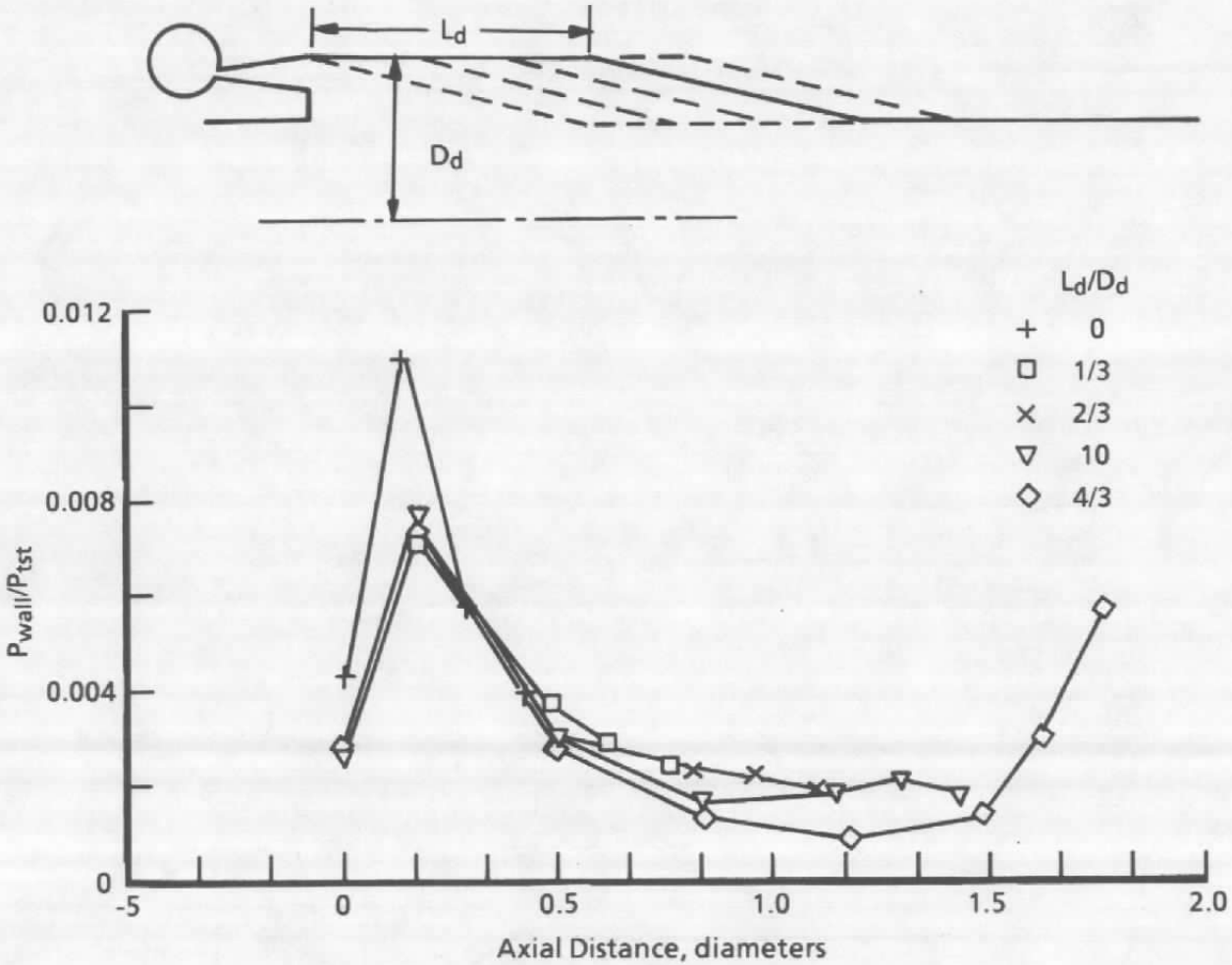

Figure 22. Effect of throat location on wall pressure profile.

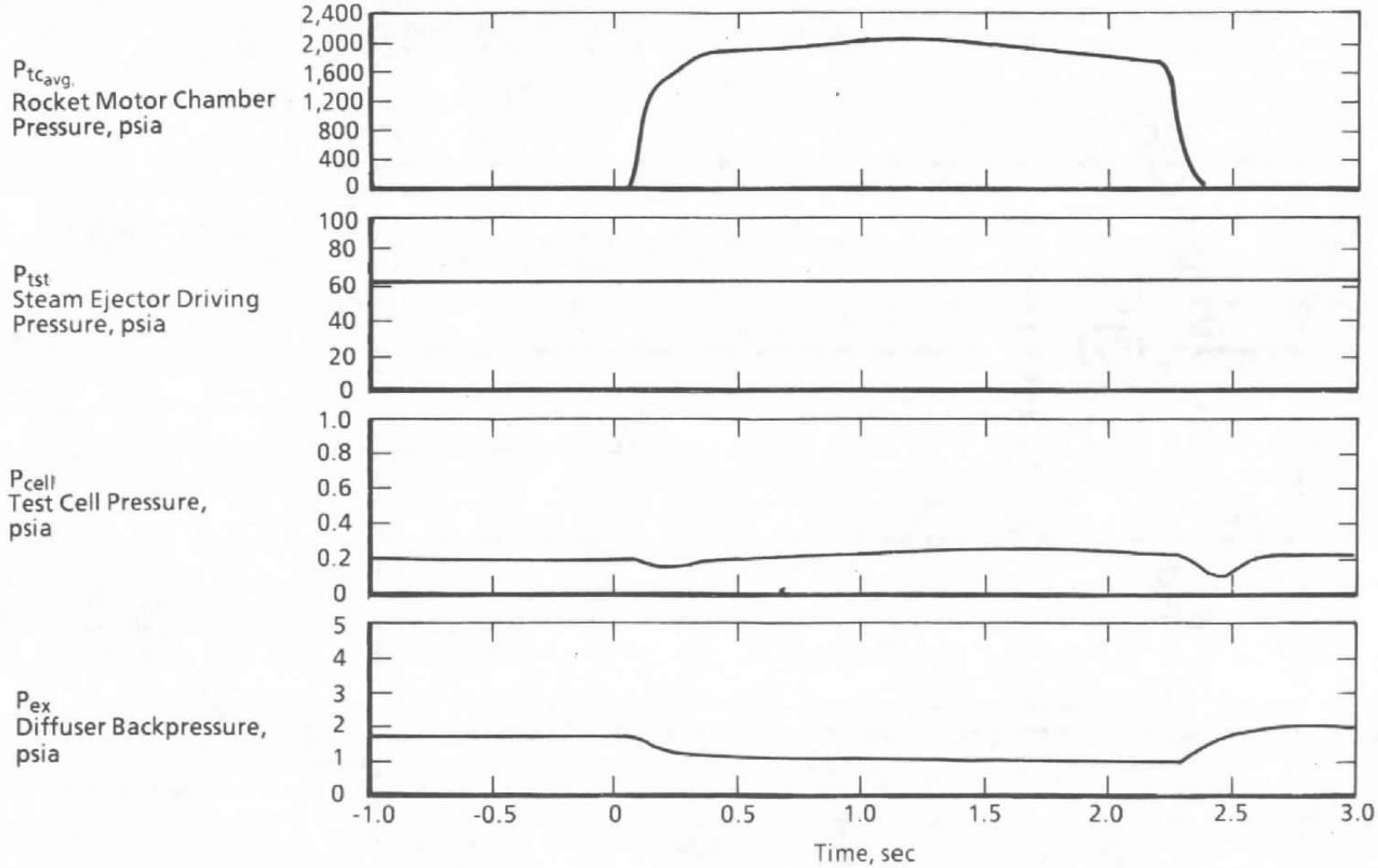

Figure 23. Rocket test results for Configuration 5 at low steam and exit pressures—started diffuser.

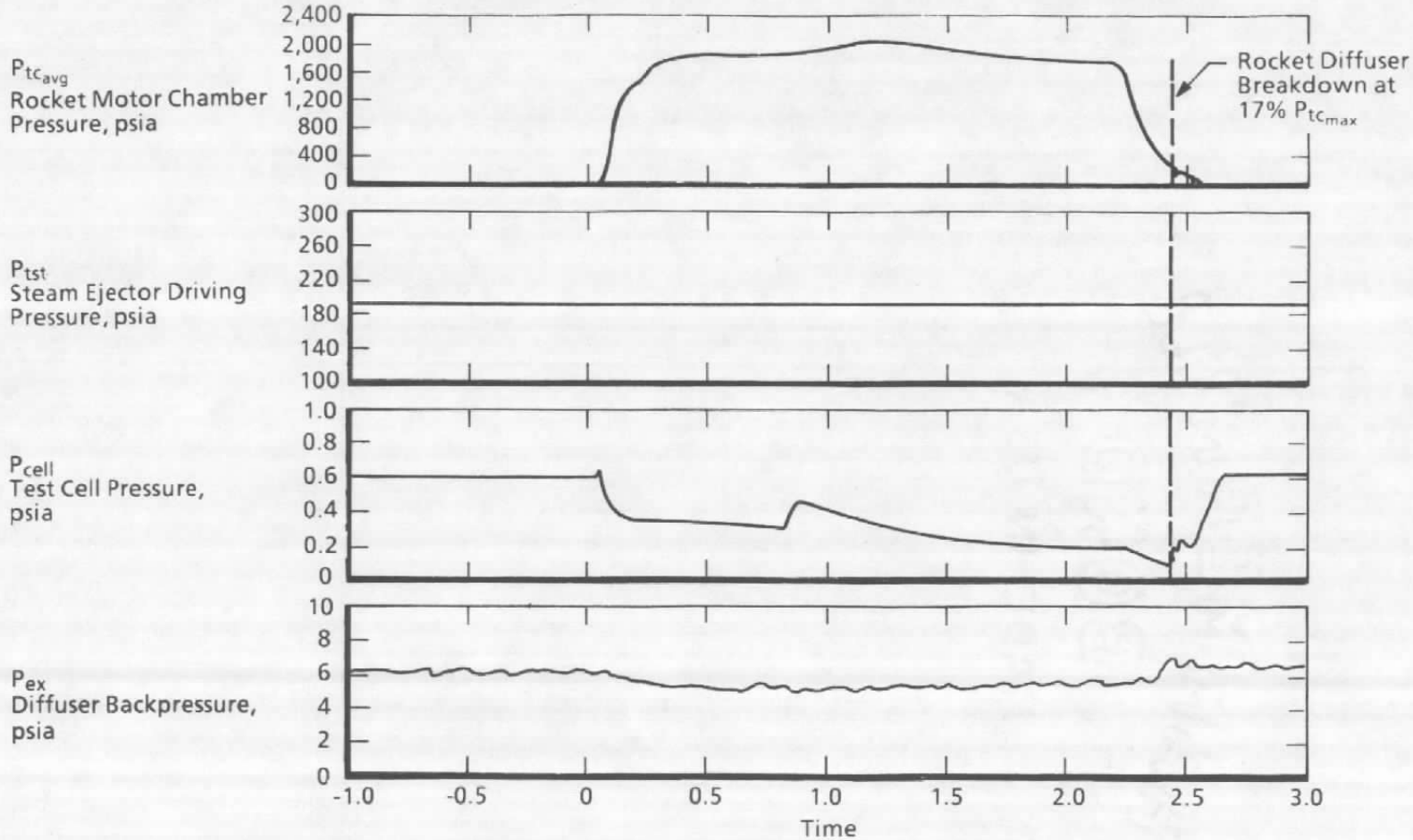

Figure 24. Rocket test results for Configuration 5 at high steam pressure and started diffuser.

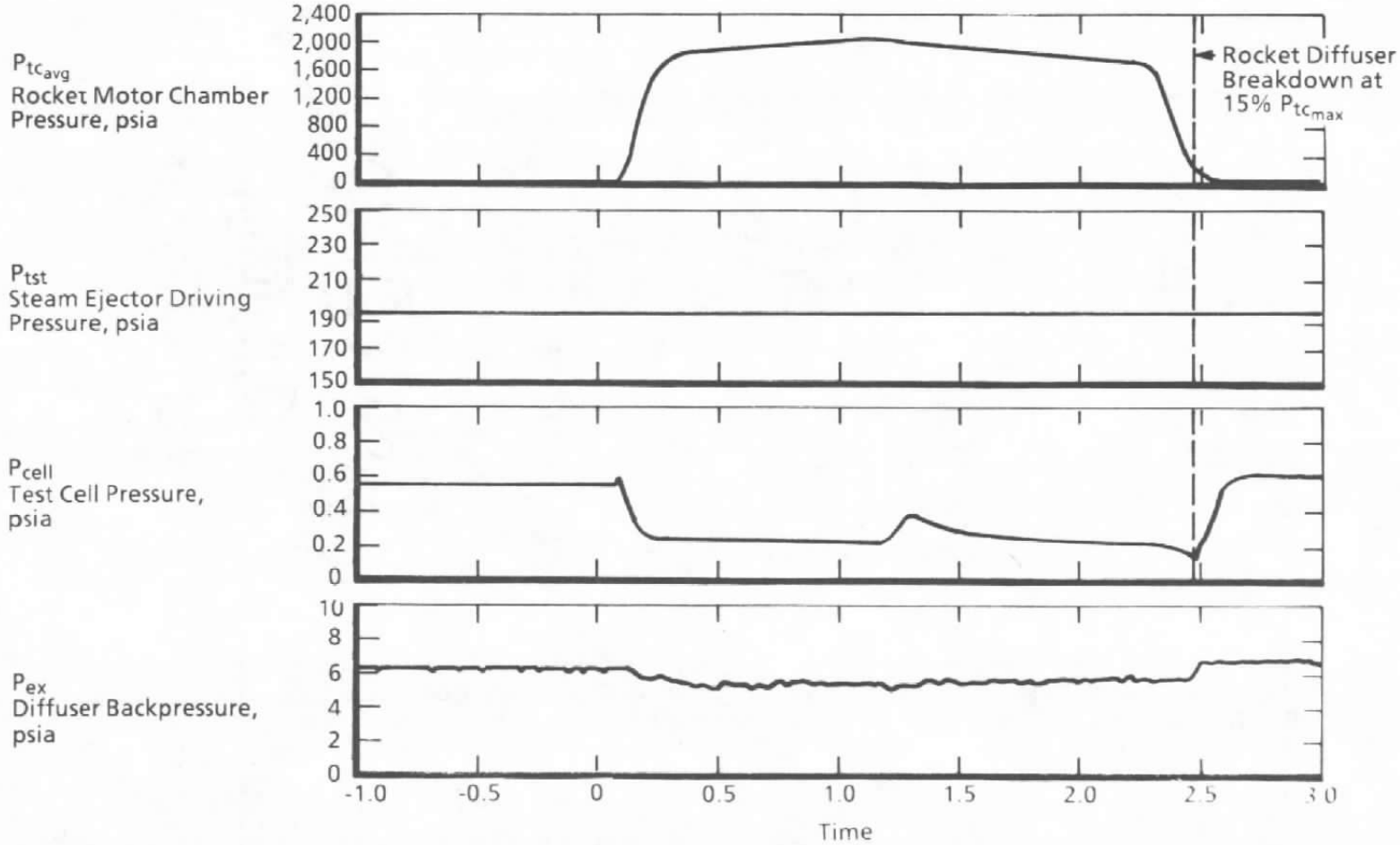

Figure 25. Rocket test results for Configuration 4 at high steam pressure and started diffuser.

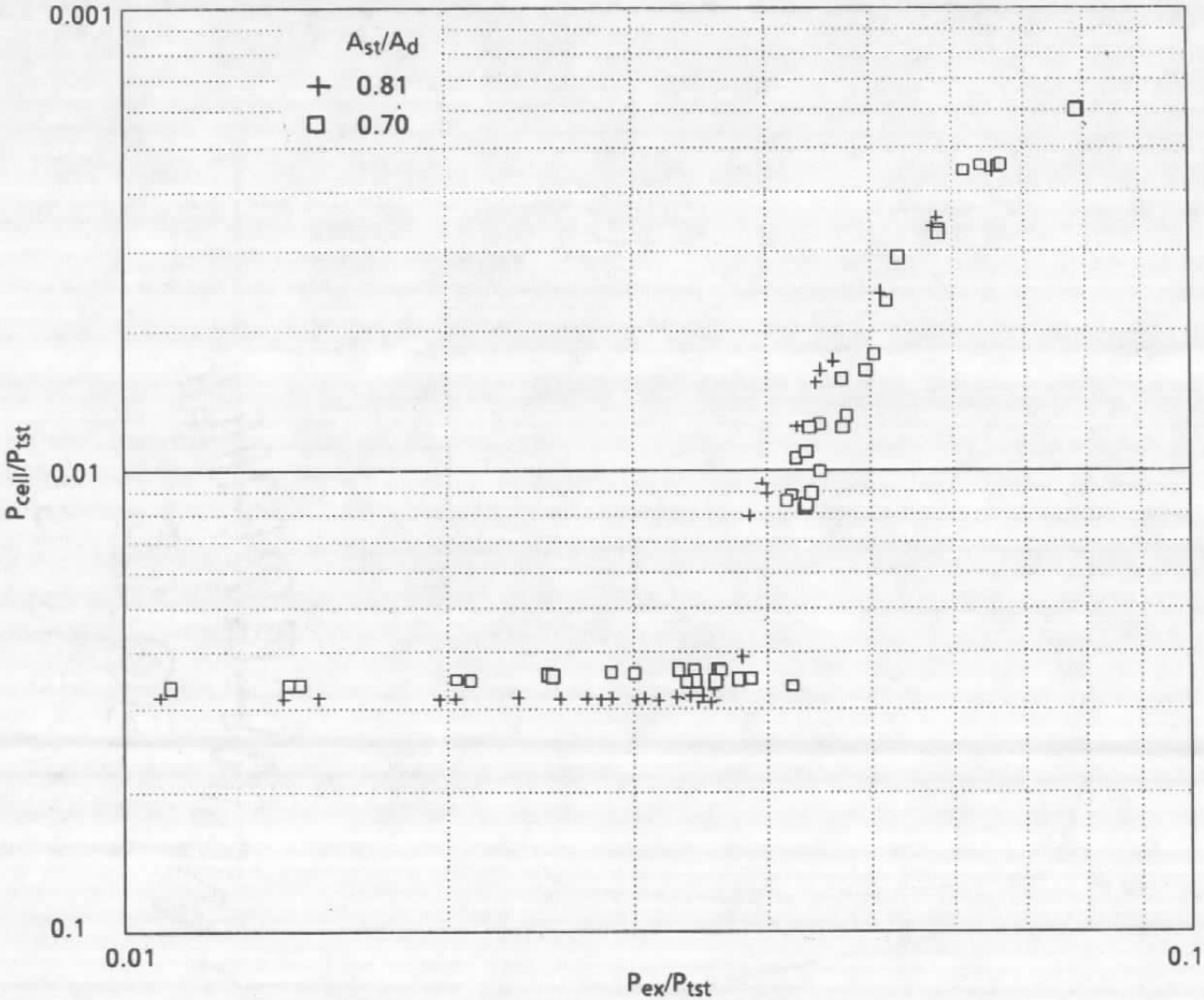

Figure 26. Effect of contraction ratio on ejector breakdown curve.

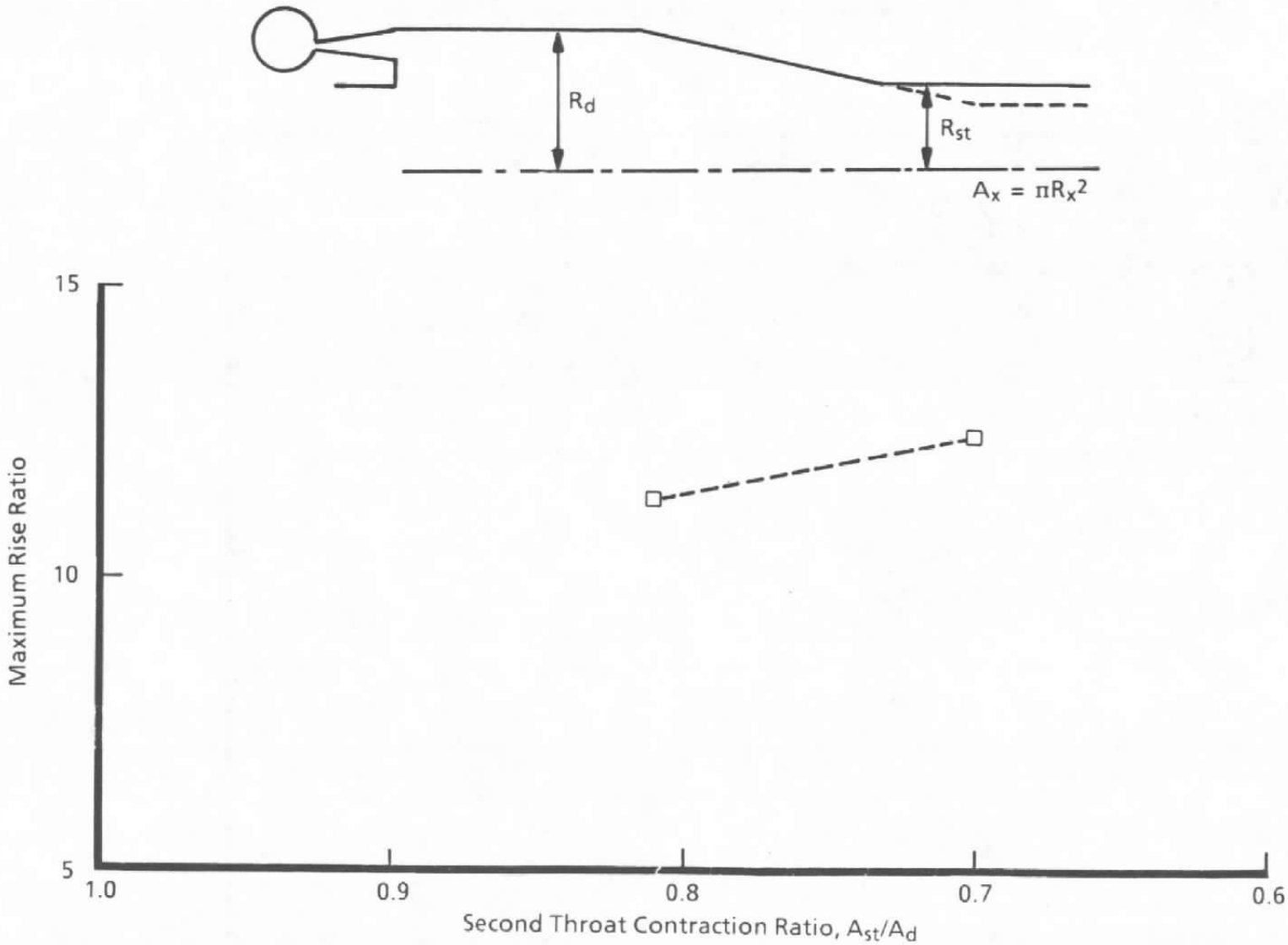

Figure 27. Effect of contraction ratio on maximum rise ratio.

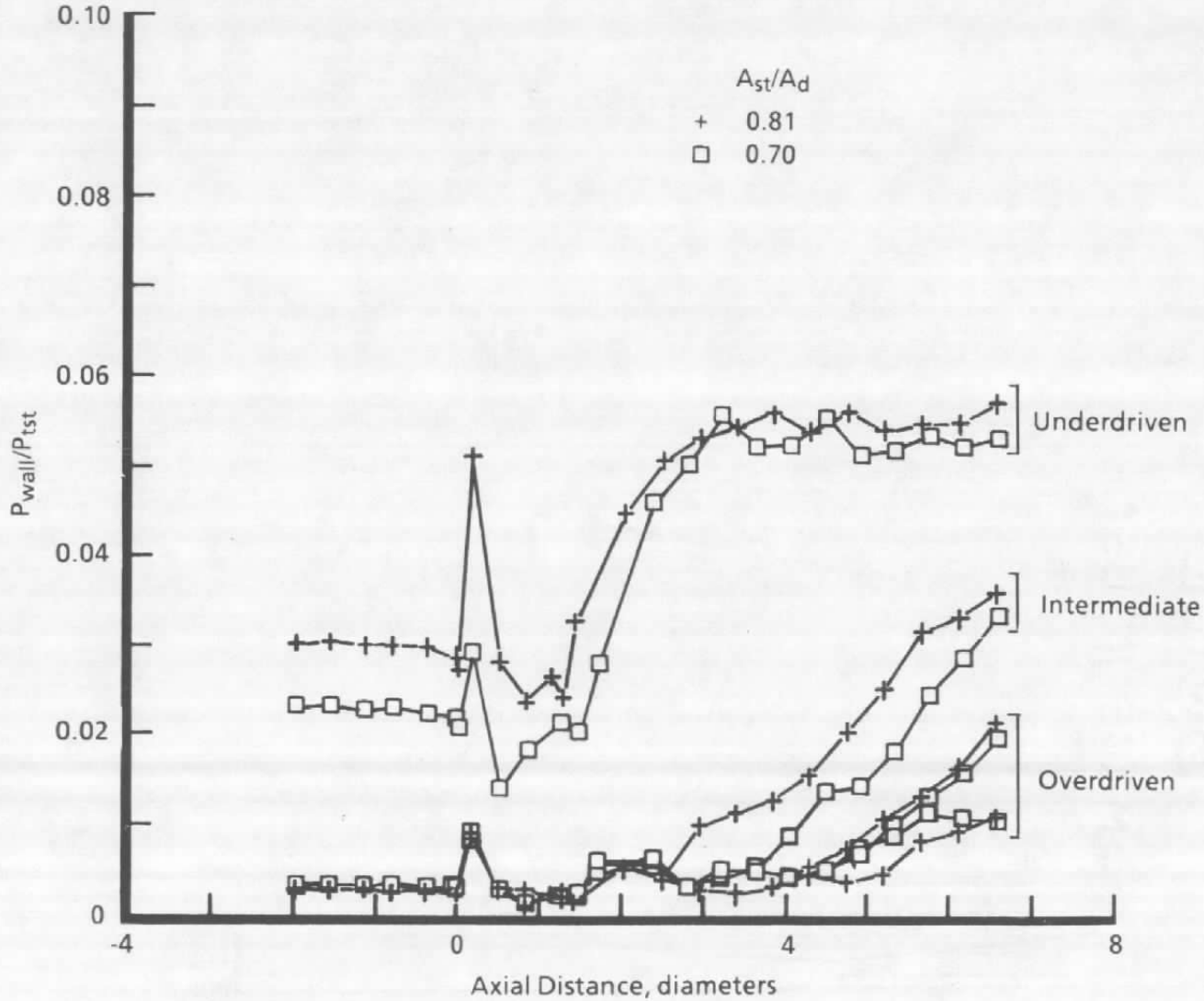

Figure 28. Effect of contraction ratio on wall pressure profile.

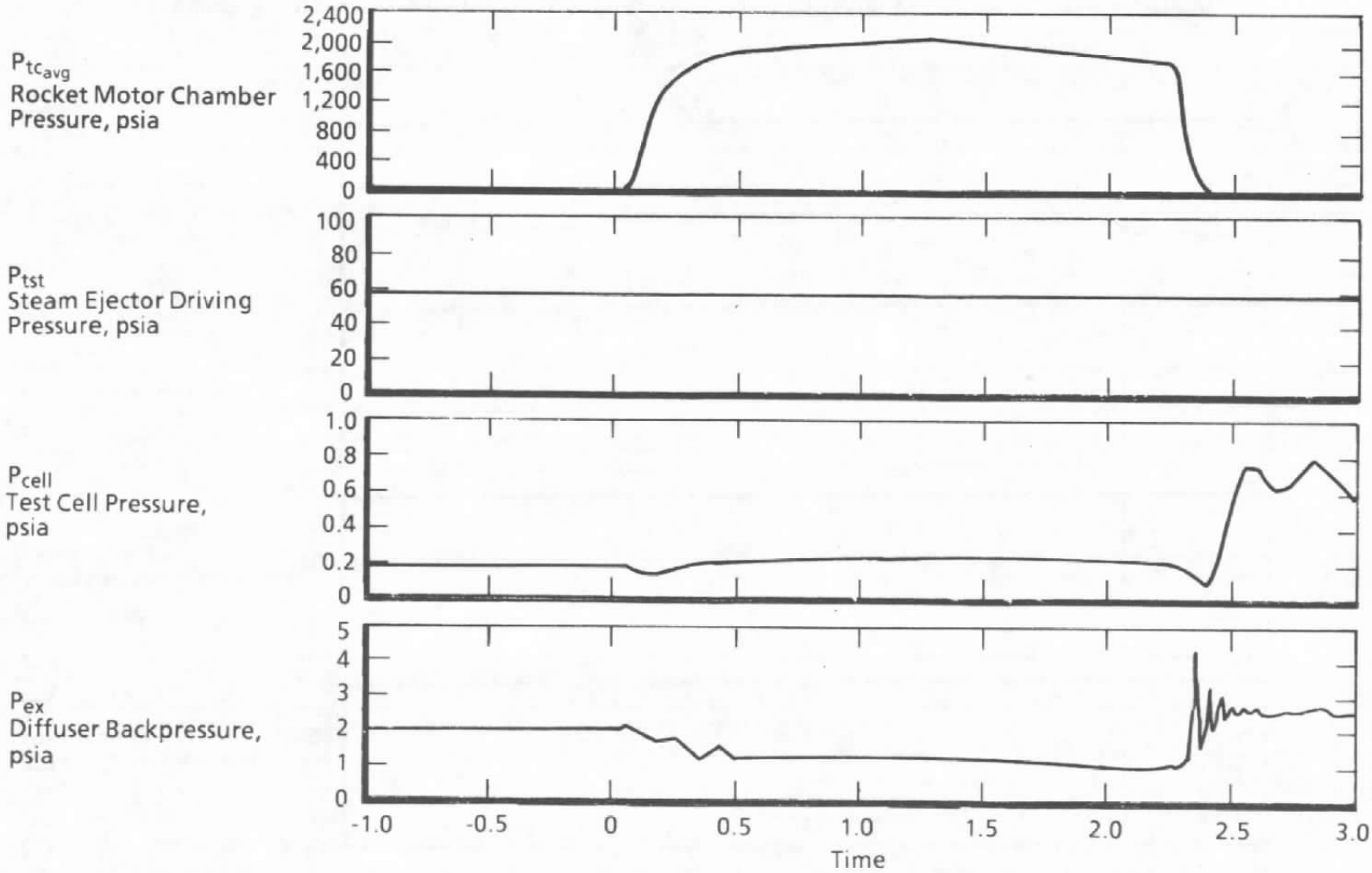

Figure 29. Rocket test results for Configuration 6 at low steam and exit pressures—started diffuser.

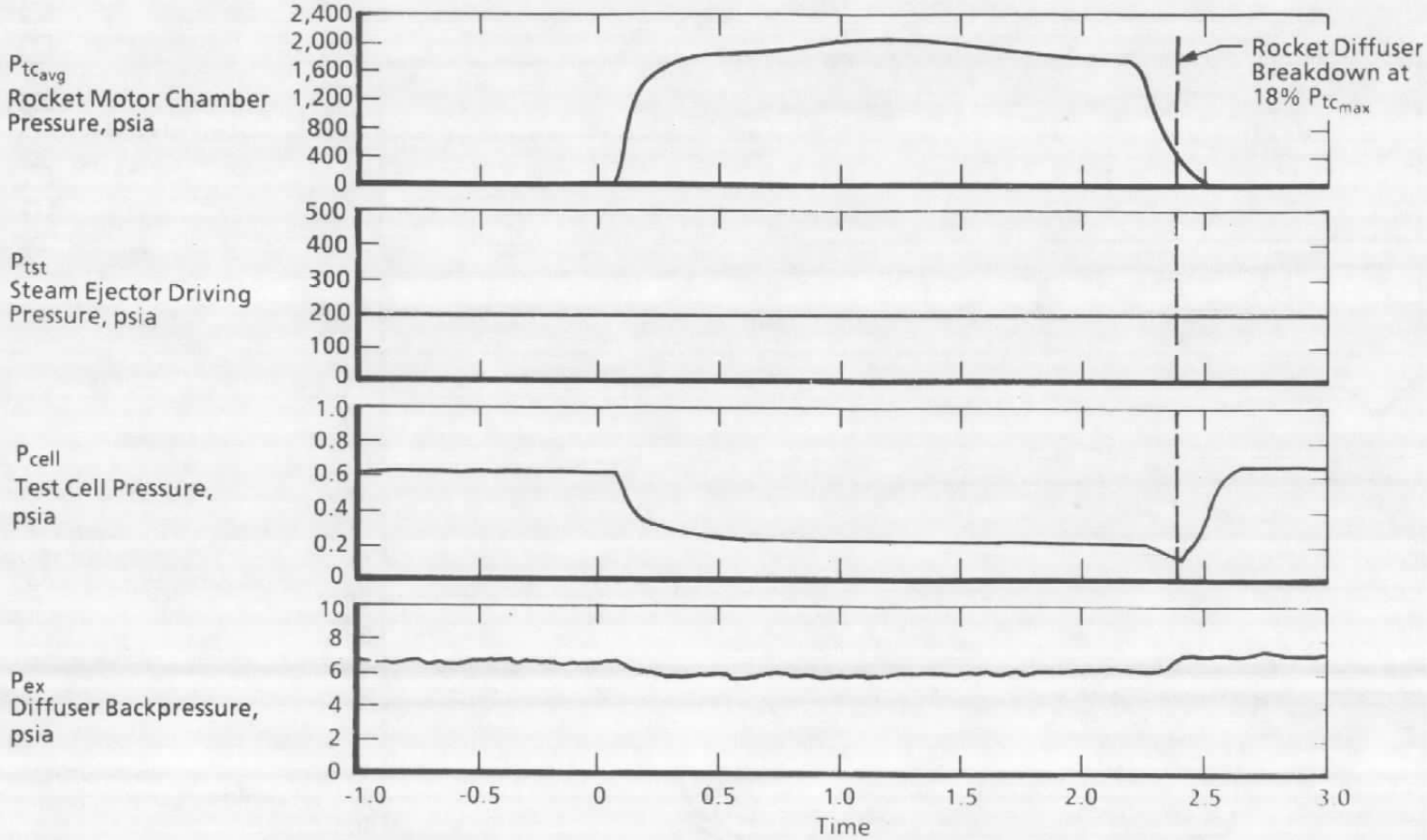

Figure 30. Rocket test results for Configuration 6 at high steam pressure and started diffuser.

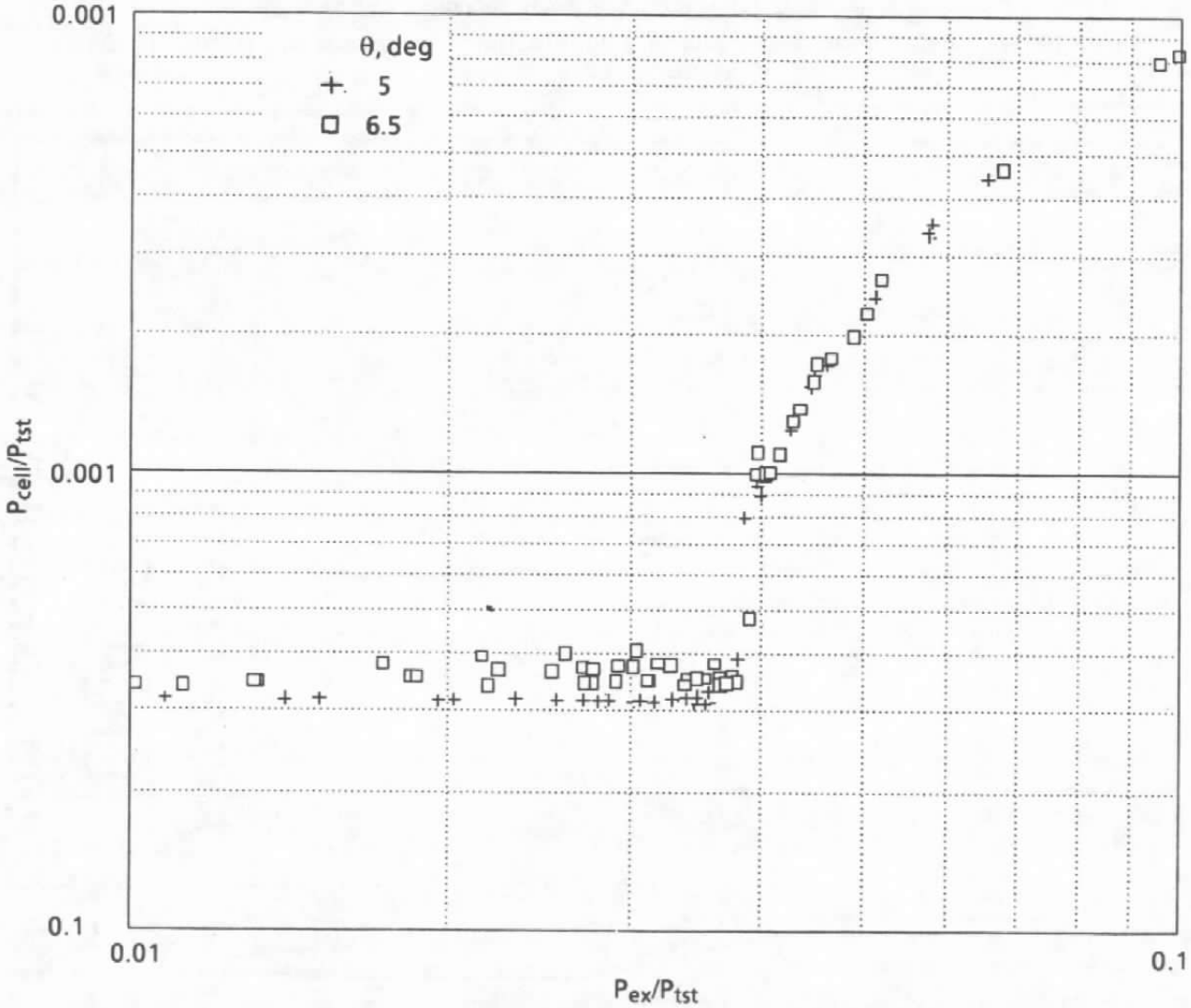

Figure 31. Effect of ramp angle on ejector breakdown curve.

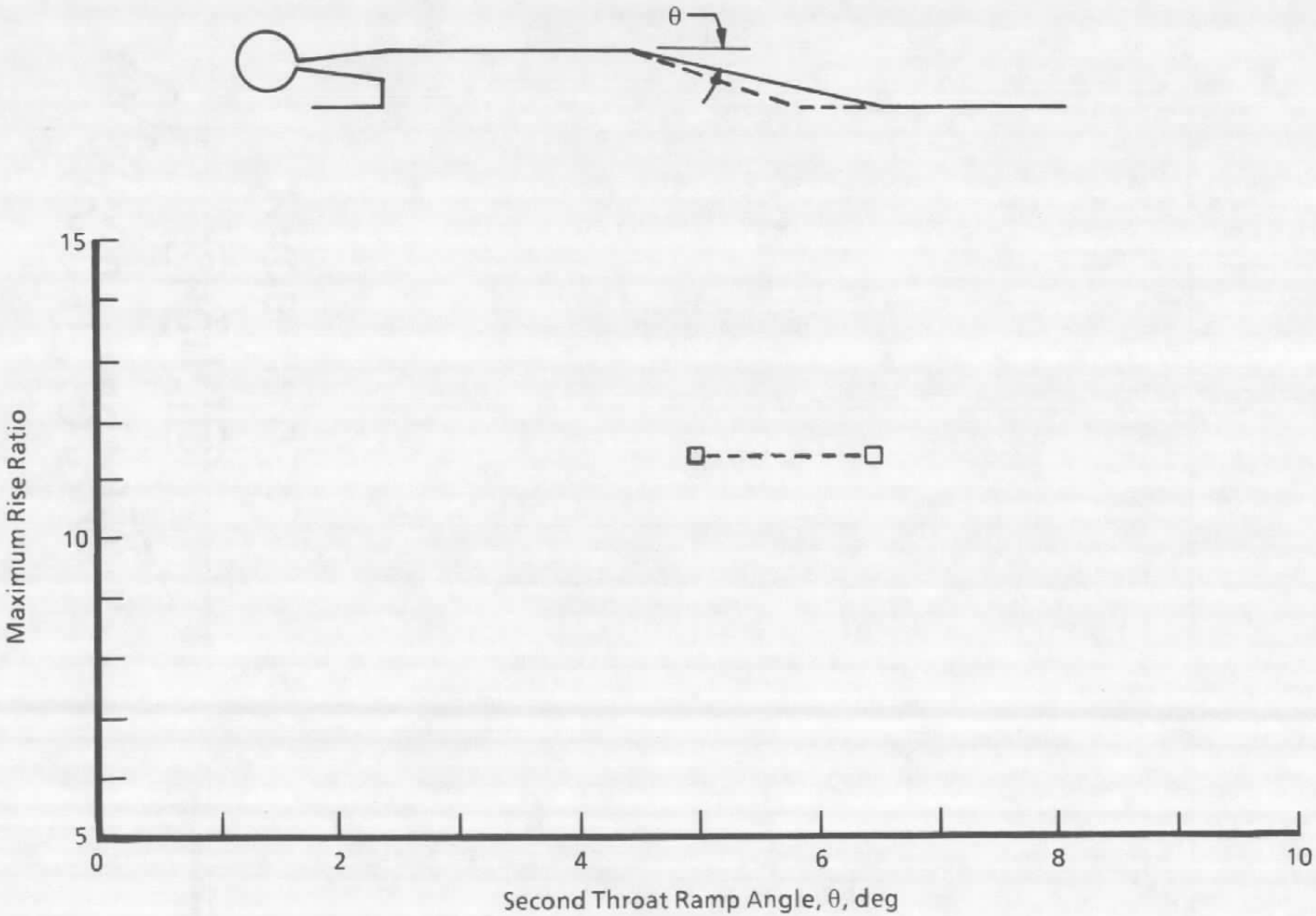

Figure 32. Effect of ramp angle on maximum rise ratio.

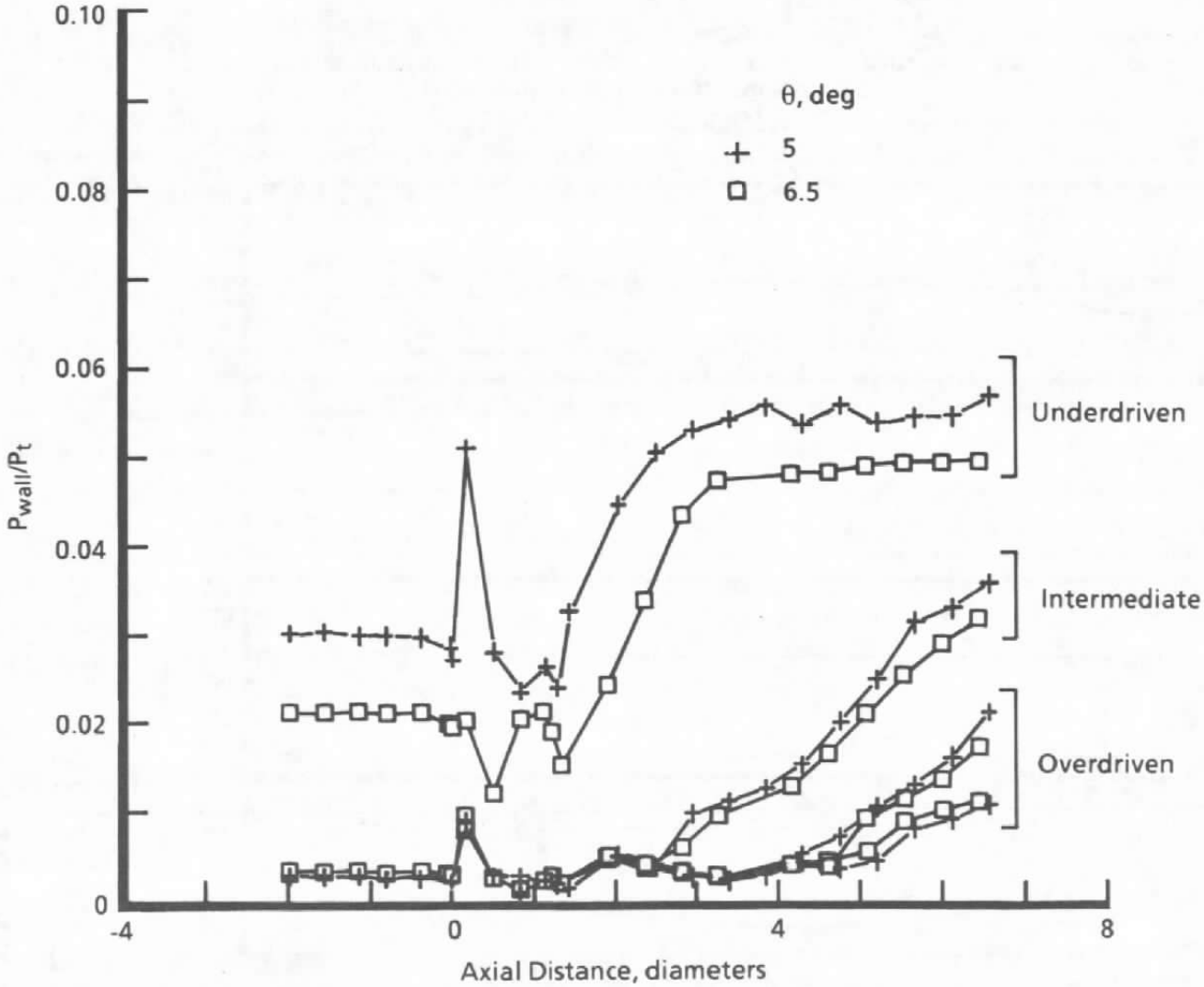

Figure 33. Effect of ramp angle on wall pressure profile.

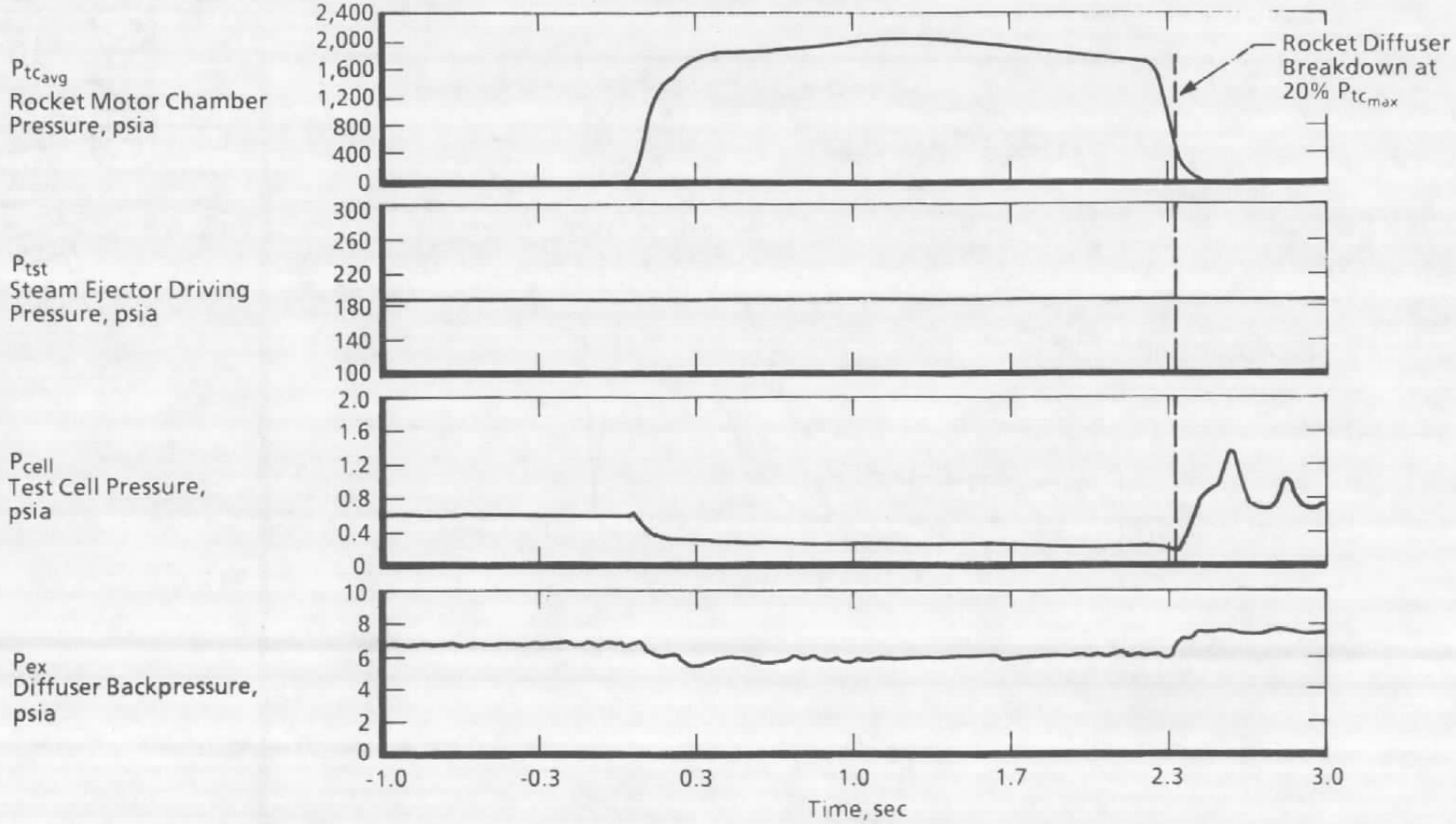

Figure 34. Rocket test results for Configuration 7 at high steam pressure and started diffuser.

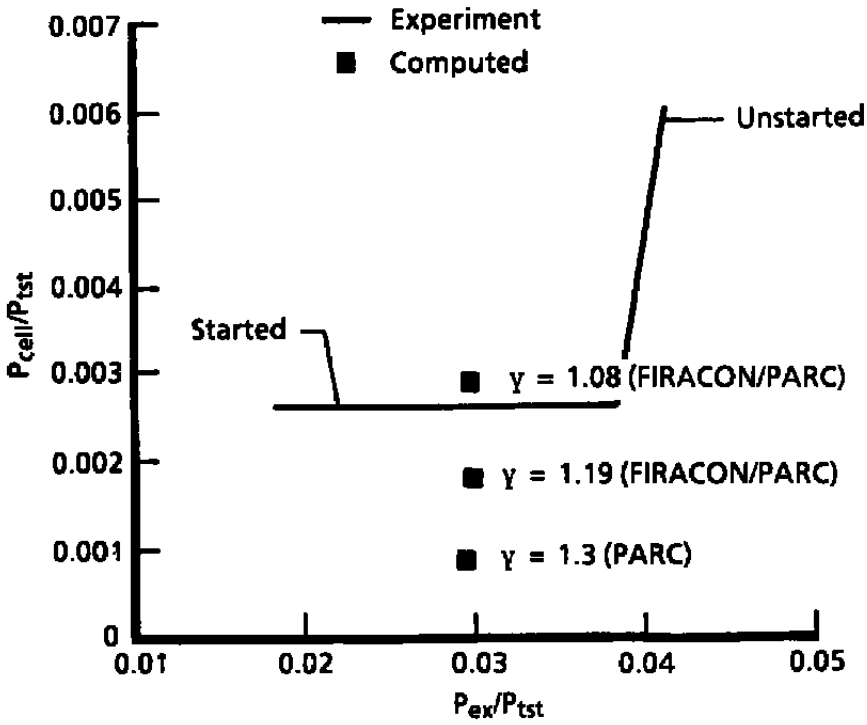

Figure 35. Analytical code calibration results.

Table 1. Ejector Configurations

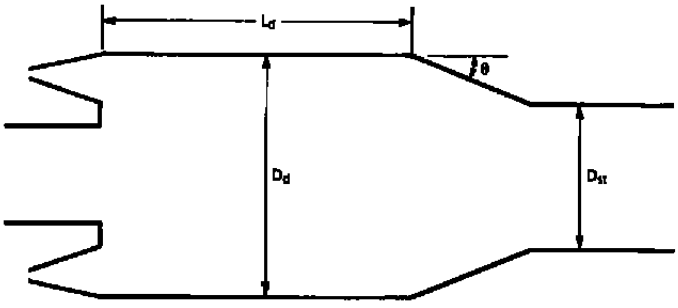

Configuration Designation	L_d/D_d	A_{st}/A_d*	Θ, deg
Baseline	1.000	0.812	5.0
2	0	0.812	5.0
3	0.333	0.812	5.0
4	0.667	0.812	5.0
5	1.333	0.812	5.0
6	1.000	0.700	5.0
7	1.000	0.812	6.5

* $A_{st}/A_d = (D_{st}/D_d)^2$

Table 2. Measurement Uncertainties*

Parameter	Description	Bias (B)	Precision (S)	Uncertainty† (U)
Pcell1 - Pcell3	Test cell pressure	±1.4	±0.3	±2.0
Pwall1 - Pwall6	Rocket diffuser wall static pressure	±0.035 psia	±0.0075 psia	±0.05 psia
Pwall7 - Pwall27	Ejector diffuser wall static pressure	±2.0	±0.5	±4.0
Ptc	Motor chamber pressure	±1.4	±0.5	±4.0
Ptex1 - Ptex6	Ejector diffuser exit pitot pressure	±1.4	±0.3	±2.0
Pseex	Ejector diffuser exit static pressure	±1.4	±0.3	±2.0
Ptst1, Ptst2	Steam manifold pressure	±1.4	±0.3	±2.0
Pnoz	Ejector nozzle wall static pressure	±2.0	±0.5	q±4.0
Pduct1	Ejector backpressure	±1.4	±0.3	±2.0
Ttst	Steam manifold temperature	±(0.8°F + 0.38 percent Reading)	±0.6°F	±(2.0 + 0.38 percent Reading)

* Bias, precision, and uncertainty are all percent of reading unless otherwise noted.
† $U = (B + t_{95}S)$

Table 3. Ejector Performance Summary

Configuration Designation	$\left.\frac{P_{ex}}{P_{cell}}\right]_{max}$	$\left.\frac{P_{cell}}{P_{tst}}\right]_{min}$	$\left.\frac{P_{ex}}{P_{tst}}\right]_{bd}$	K_{isen}	K_{ns}
Baseline					
-February	12.0	0.0030	0.036	2.14	0.79
-September	11.3	0.0032	0.036	2.29	0.79
2	7.2	0.0050	0.036	3.57	0.79
3	12.7	0.0031	0.037	2.07	0.81
4	11.9	0.0031	0.037	2.21	0.81
5	10.9	0.0034	0.037	2.43	0.81
6	12.7	0.0033	0.042	2.36	0.80
7	11.9	0.0032	0.038	2.29	0.83

bd = at breakdown

Table 4. Point Correlation for Figures 9-10, 13-15

Point Label	P_{ex}	P_{tst}	P_{ex}/P_{tst}
A	2.04	189	0.011
B	2.10	103	0.020
C	2.00	60.2	0.033
D	4.22	99.1	0.043
E	4.17	63.8	0.065

NOMENCLATURE

A_d/A^*	Ratio of diffuser to nozzle throat areas
AEDC	Arnold Engineering Development Center
A_{st}/A_d	Contraction ratio of second throat diffuser, i.e., ratio of final diffuser area to initial area
BATES	Ballistic Test and Evaluation System
D_d	Ejector diffuser diameter at nozzle exit plane, in.
D_{st}	Ejector diffuser diameter at exit, in.
ETF	Engine Test Facility
GN_2	Gaseous nitrogen
L_d/D_d	Ratio of length of diffuser constant area section to diameter, upstream of second throat
K_{isen}	Ratio of actual normalized cell pressure for the started ejector to the isentropic static to total pressure ratio for the same area ratio
K_{ns}	Ratio of actual normalized maximum exit pressure to the compressible flow normal shock approximation
$\dot{m}$	Mass flow rate, lbm/sec
NIST	National Institute of Standards and Technology, formerly the National Bureau of Standards
$(P/P_t)_{isen}$	Pressure ratio calculated using ideal gas, isentropic, compressible flow equations
$(P_2/P_{t1})_{ns}$	Normal shock downstream static to upstream total pressure ratio
P_{cell}	Test cell pressure, psia

P_{cell-n}	Test cell pressure measurements, psia (n = 1-3)
P_{duct-n}	Transition duct static pressure measurement, psia (n = 1-3)
P_{ex}	Average of Pduct1 and Pduct2, psia
P_{noz}	Ejector nozzle wall static pressure, psia
P_{seex}	Ejector diffuser exit wall static pressure measurement, psia
P_{tc}	Rocket motor chamber pressure, psia
P_{tex}	Average of ejector diffuser exit pitot pressure probe measurements, psia
P_{tex-n}	Ejector diffuser exit total pressure probe measurement, psia (n = 1-6)
P_{tst}	Average of Ptst1 and Ptst2, psia
P_{tst-n}	Steam ejector manifold pressure measurements, psia (n = 1,2)
P_{w-n}	Diffuser wall pressure, psia (n = 1-27)
R	Gas constant, ft-lbf/lbm - °R
r_d	Ejector diffuser exit radius, in.
t	Time, sec
T	Temperature, °R
T_{tst}	Steam ejector manifold temperature, °R
V	Volume
γ	Ratio of specific heats
θ	Second throat ramp angle, deg